Elasmobranch Gill Structure

Chapter · January 2016

DOI: 10.1016/B978-0-12-801289-5.00003-1

1 author:

Nicholas C. Wegner
National Marine Fisheries Service
60 PUBLICATIONS **1,316** CITATIONS

SEE PROFILE

3

ELASMOBRANCH GILL STRUCTURE

NICHOLAS C. WEGNER

1. Introduction
2. Overview of the Elasmobranch Gill
3. Evolution of the Gill: Elasmobranch Gill Structure in Relation to Other Fishes
4. Elasmobranch Versus Teleost Ventilation
5. Details of the Elasmobranch Gill
   5.1. Gross Morphology – Unique Features
   5.2. Gill Vasculature
   5.3. The Gill Epithelium
6. Diversity in Elasmobranch Gill Dimensions and Morphology
   6.1. Gill Arches
   6.2. Gill Morphometrics
   6.3. Theory on Elasmobranch Gill Dimensions and Limits to Gill Diffusion Capacity
   6.4. Scaling
   6.5. Adaptations for Fast Swimming
   6.6. Adaptations for Hypoxia
   6.7. Adaptations for Freshwater
   6.8. Adaptations for Feeding – Gill Rakers
7. Conclusions

As in other fishes, the gills of elasmobranchs are a critical interface between the internal and external environments and play vital roles in gas exchange, ion and pH balance, and the excretion of nitrogenous waste. Although the functional unit of the fish gill (the gill filament) has remained structurally and functionally intact throughout the course of fish evolution and diversification from lampreys to teleosts, the elasmobranch gill has a number of largely unique features. Perhaps most notably is the connection of the gill filaments to interbranchial septa, which affects not only the flow of water through the gills, but may provide a number of specific advantages and disadvantages to elasmobranch respiration. This chapter discusses both the structural similarities and differences of the elasmobranch gill in comparison to other fish groups and describes the breadth of structural

Physiology of Elasmobranch Fishes:
Structure and Interaction with Environment: Volume 34A
FISH PHYSIOLOGY

DOI: http://dx.doi.org/10.1016/B978-0-12-801289-5.00003-1

branchial diversity within elasmobranchs, ranging from deep-water sharks and rays with six or seven pairs of gill arches to surface-oriented giants that use specialized gill rakers to sieve micro-sized prey out of the water.

1. INTRODUCTION

Due to its multiple functions in gas exchange, ion and pH balance, and nitrogenous waste excretion, many comparative physiologists consider the fish gill as one of the most complex animal organs. This chapter focuses on the structure of the elasmobranch gill, which in a volume dedicated to the physiology of sharks, rays, and skates, provides needed insight into various life-sustaining processes that are discussed in other chapters. While the origin of the term "elasmobranch" (which is derived from their unique gill morphology) dates back to at least the 1870s, and the description of shark gills goes back much further, it was not until the second half of the twentieth century that many aspects of the elasmobranch gill were understood. Indeed, arguments persisted into the 1970s as to the basic path of ventilatory water over the respiratory surfaces, and the elasmobranch gill circulation was not well studied until the 1980s. Only in recent years have we begun to understand the functional role of the gill in the exchange of ions between the blood and the water. In comparison to the gills of teleosts, much less is still known about elasmobranch gill structure and function. This chapter synthesizes the available knowledge on elasmobranch gill structure and morphology, building off of previous reviews (Butler and Metcalfe, 1988; Butler, 1999) and highlights needs for areas of future research.

2. OVERVIEW OF THE ELASMOBRANCH GILL

A series of detailed schematics of elasmobranch gill morphology, from an overview of the entire branchial apparatus down to the fine structure of the respiratory surfaces, is presented in Fig. 3.1. This figure identifies most of the structural and morphological components of the gills and ventilatory-stream pathway and is thus meant to serve as a reference or guide throughout the chapter.

Literally translated from its Greek roots, "elasmobranch" means "strap" or "plate gill" which refers to the unique attachment of the gill filaments to a plate-like interbranchial septum that extends from each gill (=branchial) arch in the posterior-lateral direction (lateral view shown in Fig. 3.1A). In most elasmobranchs, there are five gill-bearing arches on each side of the

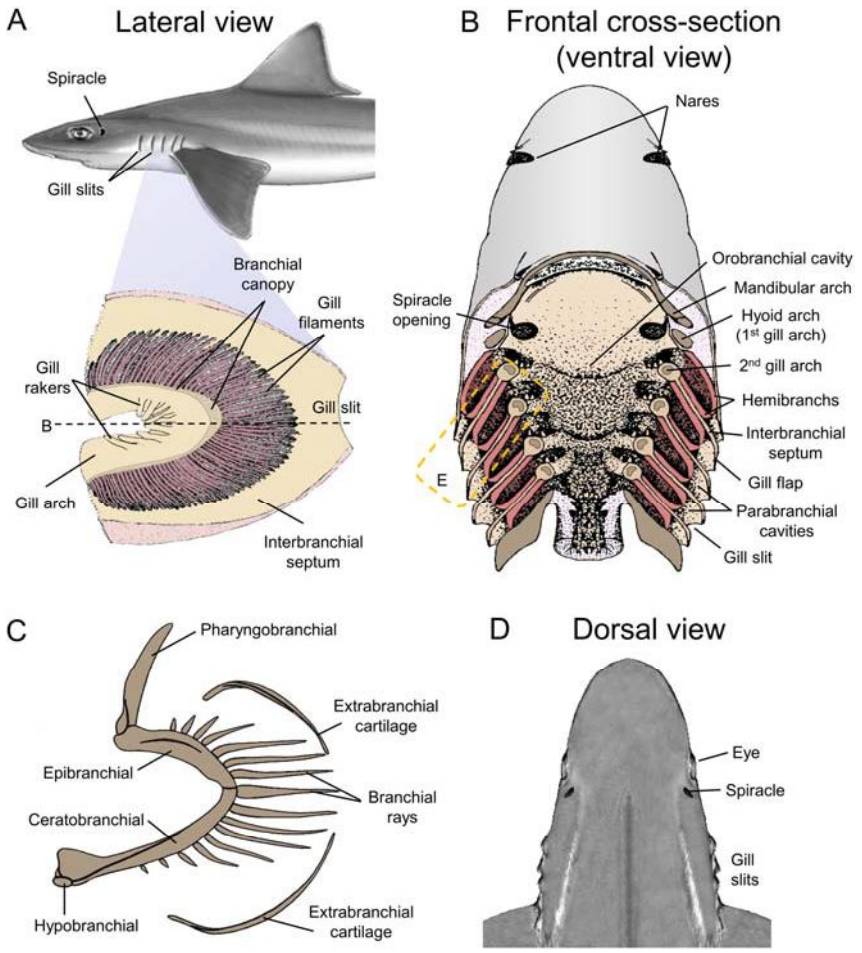

Figure 3.1. Schematic overview of elasmobranch branchial morphology. (A) Enlarged lateral view of the anterior hemibranch of a single gill arch. (B) Ventral view (looking toward the roof of the orobranchial cavity) of a frontal cross-section through the branchial region showing the relationship of the oro- and parabranchial cavities and gills. (C) Lateral view of the main skeletal elements of the gill arch. (D) Dorsal view of an elasmobranch showing the relative position of the spiracles. (E) Magnified cross-section of two gill holobranchs from the dashed box in (B) showing the positioning of the interbranchial septum, gill filaments, and lamellae. (F) Enlarged view of box in (E) showing a cross-section through two gill filaments and the pathway of water past the gill lamellae and into the septal channels. (G) Cross-section through three gill lamellae from (F) showing the blood channels formed by pillar cells. (H) Magnified view of dashed box in (G) showing the details of the lamellar blood channels and gill epithelium. ABA, afferent branchial artery; AFA, afferent filament artery; EBA, efferent branchial artery; EFA, efferent filament artery; IMC, inner marginal channel; MRC, mitochondrion-rich cell; RBC, red blood cell. Drawings based largely on or modified from Daniel (1934), Kempton (1969), Mallatt (1984), Palzenberger and Pohla (1992), and Wegner (2011).

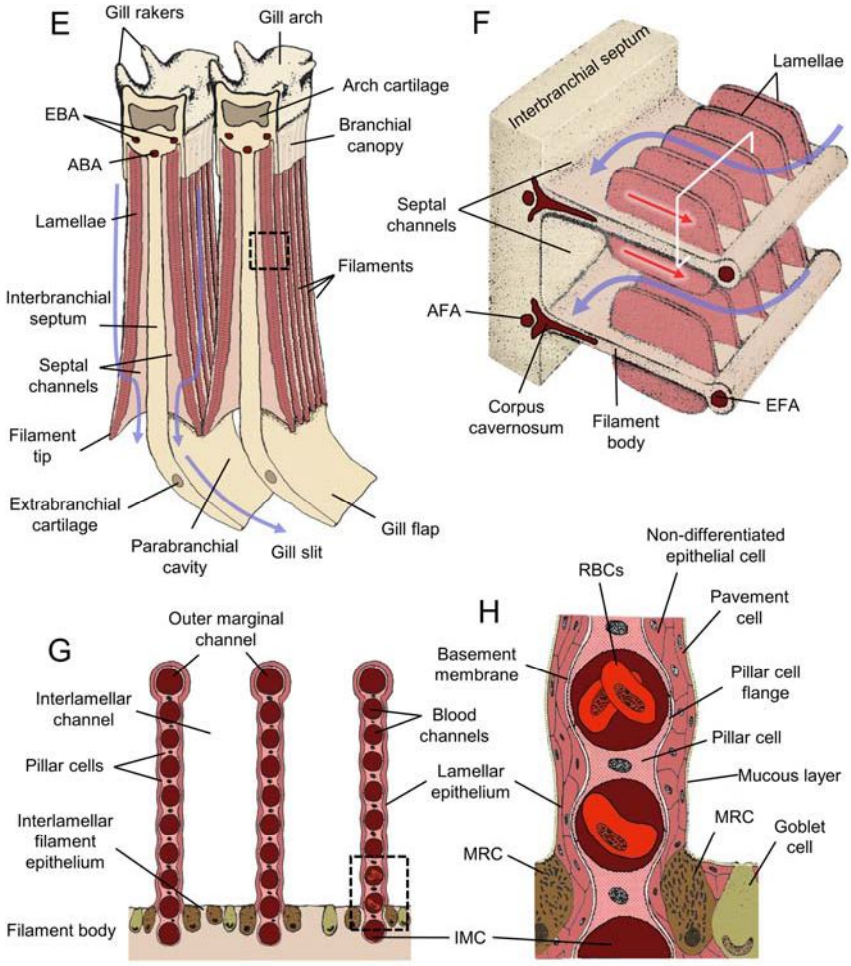

Figure 3.1. (Continued)

orobranchial cavity (frontal plane cross-section shown in Fig. 3.1B) with an arch-like row or stack of filaments (termed a hemibranch) on each exposed side of each septum (Fig. 3.1A shows the anterior hemibranch of a single arch). For the first gill-bearing arch (hyoid arch) there is only a single posterior facing hemibranch, while on arches 2–5 there is usually both an anterior and posterior hemibranch (together termed a holobranch) on each side of the septum (Fig. 3.1B). The blade-like gill filaments of each hemibranch are attached to the interbranchial septum for the majority of their lengths with just their tips extending off the septum in order to approximate the filament tips of the

opposing gill arch (Fig. 3.1A, B, and E). This approximation of the filament tips creates a general sieve or curtain through which the ventilatory stream must pass (Fig. 3.1B and E). Water flows from the orobranchial cavity (medial and anterior to the gill sieve) through the gill filaments and into parabranchial cavities, which are formed by the extension of the fleshy interbranchial septa past the filament tips to the lateral edge of the body (Fig. 3.1B and E). Here the septa [composed of muscular and connective tissue and supported by a number of cartilaginous rays emanating from each gill arch (Fig. 3.1C)] form the gill flaps, between which are the easily recognized gill slits characteristic of all elasmobranchs (Fig. 3.1A, B, D, and E).

As in most other fishes, each side of each elasmobranch filament supports a row of lamellae, which have a flat, plate-like morphology (Fig. 3.1F) that provides a large surface area and short diffusion distance for effective gas exchange between the blood and water. Blood flow through the lamellae is generally in the opposite direction of the ventilatory water stream (Fig. 3.1F), thereby creating a counter-current loading mechanism that is effective at allowing a high proportion of dissolved environmental oxygen to diffuse into the blood stream. Pillar cells, which extend across the blood lumen and connect the respiratory epithelium on either side, direct the flow of blood through the lamellae (Fig. 3.1G and H). The lamellar water–blood barrier is typically composed of one to three layers of epithelial cells, a basement membrane, and the flanges of pillar cells that form the inner lining of the blood lumen wall (Fig. 3.1H). In many species, the lamellar epithelium may contain specialized epithelial cells such as mitochondrion-rich cells (MRCs) (involved in ion and pH balance) or goblet cells (involved in mucus production); however, these specialized cells are necessarily large and thus, in most elasmobranchs (and other fishes), are usually found in greatest density within the nonrespiratory filament epithelium (Fig. 3.1G and H).

3. EVOLUTION OF THE GILL: ELASMOBRANCH GILL STRUCTURE IN RELATION TO OTHER FISHES

In order to best understand how the elasmobranch gill is both specialized and potentially limited, a basic overview of the evolutionary history of the gill and its basic structure in other fish groups is useful. There are numerous reviews on comparative aspects of gill morphology and respiration from hagfishes to teleosts (see Hughes, 1984; Wilson and Laurent, 2002; Evans et al., 2005; Graham, 2006).

Fish gills are generally thought to be derived from a series of paired pouches on the lateral walls of the pharynx that open externally to slits. Based

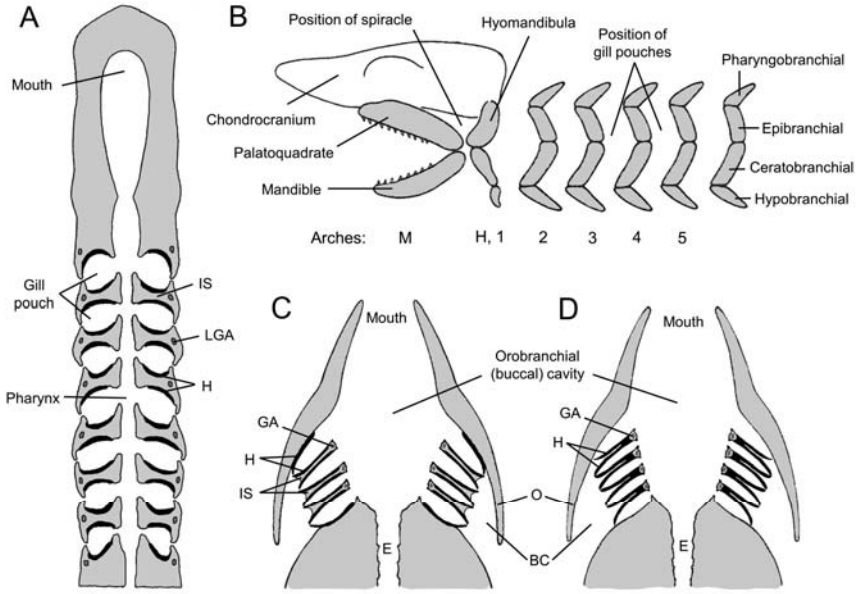

Figure 3.2. Stylized renderings of the branchial region for a(n) (A) lamprey, (B) elasmobranch, (C) holocephalan, and (D) teleost. (A, C, and D) are frontal cross-sections for comparison with that of an elasmobranch in Fig. 3.1B. (B) is a lateral view of the gill arch and jaw skeletal elements for an elasmobranch. Arches are labeled as mandibular (M), hyoid (H, 1) or by number. BC, branchial cavity; E, esophagus; GA, gill arch; H, hemibranch; IS, interbranchial septum; LGA, lateral gill arch; O, operculum. Drawings based on or modified from Hildebrand and Goslow (2001) and Randall et al. (2002).

on the morphology of protovertebrates (e.g., amphioxus), gill slits likely originally evolved for filter feeding with cilia moving water through the pharynx to collect particulates to be ingested. Presumably, as these basal chordates increased in size and the pharyngeal pouches became more pronounced and involved in respiration, epithelial folds developed to increase the surface area available for gas exchange. The most basal fishes, hagfishes (Order Myxiniformes), have a series of well-developed branchial pouches on either side of the pharynx (5–14 depending on the species) that are lined with extensive epithelial folds for gas transfer: the most primitive fish gill.

The lampreys (Petromyzontiformes), which have seven paired branchial pouches, have a gill morphology generally similar to that of elasmobranchs and higher fishes with distinct hemibranchs on the anterior and posterior face of each gill pouch bearing filaments with lamellae that are similar in shape, structure, and orientation to other fishes (Fig. 3.2A). The fleshy tissue (=interbranchial septum) between successive gill pouches is hourglass shape in frontal cross-section (rather than "plate-like" as in elasmobranchs), and

thus lampreys retain pouch-like chambers similar to hagfishes (Fig. 3.2A). However, unlike hagfishes, lampreys have a pronounced skeletal support system with a cartilaginous branchial arch located lateral to each hemibranch (Fig. 3.2A); this laterally-located arch is likely homologous to the extrabranchial cartilages in elasmobranchs that run along the lateral borders of the interbranchial septa (Hughes and Morgan, 1973; Mallatt, 1984) and provide rigidity to the parabranchial cavities (Fig. 3.1C and E). This rigidity is important for the expansion of the parabranchial cavities during elasmobranch ventilation (Hughes and Ballintijn, 1965).

In elasmobranchs (and other jawed fishes), the septa and gills are supported by branchial arches located medial to the gills (Figs 3.1A–C, E and 3.2B–D). Each arch is typically composed of four cartilaginous segments, termed from dorsal to ventral: pharyngobranchial, epibranchial, ceratobranchial, and hypobranchial (Figs 3.1C and 3.2B) with the epi- and ceratobranchial typically forming the arch that bears gill filaments and with the pharyngo- and hypobranchial anchoring the arch to the roof and floor of the orobranchial cavity. The jaws of elasmobranchs and higher fishes (the agnathans, hagfish and lampreys, lack jaws) are generally thought to be derived from branchial arches that migrated forward for use in prey capture and manipulation, with the epibranchials and ceratobranchials of the mandibular arch forming the upper and lower jaws respectively and the hyoid arch moving forward to provide added support (Fig. 3.2B). The remnant of the dorsal gill slit between the mandibular and hyoid arches forms the spiracle (Fig. 3.2B), which persists in many benthic elasmobranchs (especially rays and skates) and a few primitive bony fish lineages and allows for the inspiration of water into the orobranchial cavity through openings on the dorsal-lateral surface of the head (Fig. 3.1A, B, and D) when the mouth is buried in the substrate or engaged in prey manipulation. In many species, the remnant of the posterior hemibranch of the mandibular arch (known as the pseudobranch) still exists on the dorsal lateral surface of the orobranchial cavity. The posterior hemibranch of the hyoid arch also persists in elasmobranchs and some primitive bony fishes and in many texts (including this chapter) is referred to as the first gill arch or the first arch bearing true gills (the "pseudobranch" literally meaning "false gill").

In elasmobranchs the interbranchial septum of each gill arch extends to the lateral edge of the body to form the gill flaps and gill slits (Fig. 3.1A, B, and E). In both holocephalans (=chimaeras, Order Chimaeriformes) and bony fishes, the interbranchial septa separating the gill pouches are reduced, which results in a single large branchial (opercular) cavity on either side of the buccal cavity containing all the gill hemibranchs (Fig. 3.2C and D). With reduced septa, the gills are protected laterally by a fleshy extension of the hyoid arch (chimaera) or a bony operculum

(bony fish) [these two types of protective coverings are not homologous (Hughes and Morgan, 1973)]. For chimaeras and a few basal bony fishes, the interbranchial septum extends out to or near the tips of the filaments (Fig. 3.2C), while in most teleosts the septum has been reduced to just near the origin of the filaments near their attachment to the gill arch (Fig. 3.2D). The filaments in teleosts are thus not bound to the septum for most of their length, and this has implications for both gill rigidity and the flow of water past the respiratory surfaces in comparison to the "strapped" gill configuration of elasmobranchs.

4. ELASMOBRANCH VERSUS TELEOST VENTILATION

The major biomechanical features of gill ventilation are generally consistent within jawed fishes and have been well studied in both elasmobranchs and teleosts (see for review Brainerd and Ferry-Graham, 2006; Wegner and Graham, 2010). Water typically enters the orobranchial cavity (elasmobranchs) or buccal cavity (bony fishes) through the mouth and or spiracles and is forced through the gills using a dual pumping mechanism (Hughes, 1960a,b). This includes a "force" pump (associated with the expansion and compression of the orobranchial/buccal cavity), and a "suction" pump (created by the expansion of the parabranchial cavities/branchial cavities in bony fishes). Together, the use of these two pumps results in the flow of water over the respiratory surfaces that, although often highly pulsatile, is thought to be continuous or nearly continuous in most fishes. However, some potential for back flow, or at least the stalling of flow, has been documented in some elasmobranchs (see for review Summers and Ferry-Graham, 2003). Some fishes (particularly those that are fast or continuous swimmers) are also capable of ram ventilation in which branchial flow is established via holding the mouth and gill slits ajar during forward swimming (Hughes, 1960b; Roberts, 1975). In this case, ventilatory flow past the gas exchange surfaces is generally constant (Brown and Muir, 1970; Wegner et al., 2012).

In both active (pumping) or passive (ram) ventilation, water leaving the orobranchial (buccal) cavity is forced laterally between the gill arches (sometimes referred to as gill bars) where it must turn to enter the interlamellar spaces where gas exchange occurs (Figs 3.1–3.3). In elasmobranchs, water that passes through the interlamellar channels encounters the interbranchial septum and must thus subsequently turn and follow septal channels (Fig. 3.3A and B) along the length of the filaments until it enters the parabranchial cavities and exits at the gill slits. For bony fishes, the reduction of the interbranchial septum allows water to pass through the interlamellar spaces generally unimpeded (Fig. 3.3C and D).

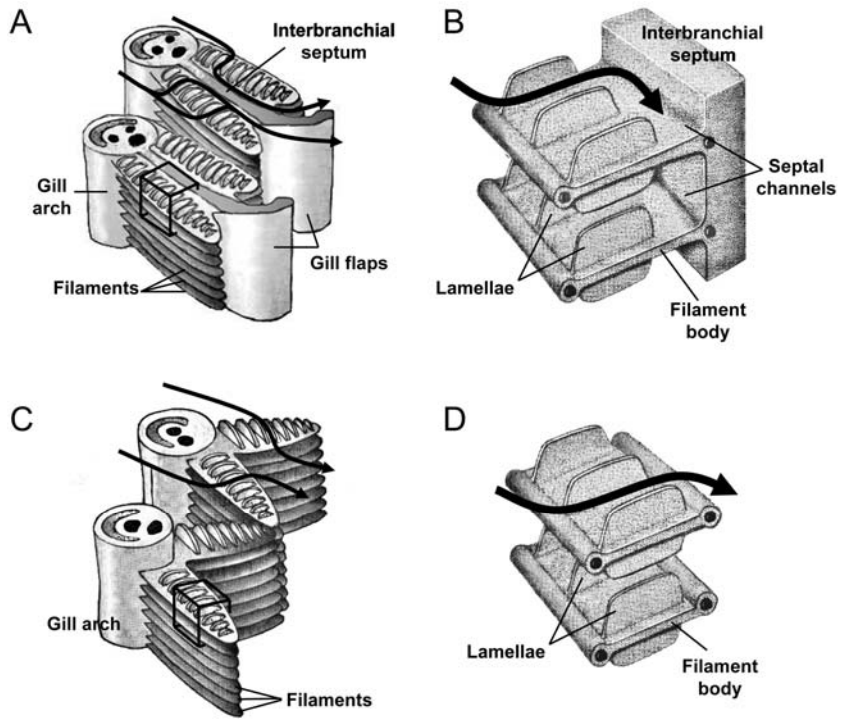

Figure 3.3. Simplified drawings of the elasmobranch (A and B) and teleost (C and D) gill. (B) and (D) are enlarged views of the boxes in (A) and (C) respectively. The path of water flow through the gills is indicated by arrows. From Wegner et al. (2012).

The strapping of the gill filaments to the interbranchial septum in elasmobranchs is potentially advantageous in providing added rigidity to the gills. Specifically, this morphological configuration would suggest that high branchial flow volumes are less likely to cause deformation of the filaments resulting in the shunting of water between adjacent filaments or opposing hemibranchs and causing a decrease in oxygen extraction efficiency. This may partially explain why a high proportion of elasmobranchs, including many generally benthic-oriented genera such as *Triakis* are capable of ram ventilation (Hughes, 1960b; Clark and Kabasawa, 1976). However, the interbranchial septum adds a site of resistance to water flow through the elasmobranch gill. Although the total pressure gradient establishing ventilatory flow across the gills (and consequently total gill resistance) is generally similar between elasmobranchs and bony fishes during both active and ram ventilation (Hughes, 1960a,b; Brown and Muir, 1970; Wegner et al., 2012), Wegner et al. (2012) calculates that in the shortfin mako, *Isurus*

oxyrinchus, up to 80% of the gill resistance results from flow through the septal channels. To compensate for this added resistance, elasmobranchs appear to have generally larger interlamellar spaces than bony fishes and consequently fewer lamellae per unit of filament length. This lower number of lamellae may impose limits to elasmobranch gill surface area and ultimately aerobic scope (Wegner et al., 2012) (see Section 6.3).

5. DETAILS OF THE ELASMOBRANCH GILL

5.1. Gross Morphology – Unique Features

While a general overview is discussed above, there are several interesting and largely unique features of the elasmobranch gill that warrant additional description, many of which are poorly studied and have largely unknown, or at least unverified, functions.

As the ventilatory stream passes the gill arches, it encounters the gill filaments and lamellae where gas exchange occurs. In addition to the interbranchial septum that binds and reinforces the trailing (water-exit) filament edge, thin, fleshy extensions of the gill arch on each hemibranch bind adjacent filaments on the leading (water-entry) edge. This results in a "branchial canopy" that can cover anywhere from just 6–8 lamellae (Donald, 1989) to up to 15–20% of the filament length nearest the arch (Figs 3.1A and E and 3.4) (Cooke, 1980; Benz, 1984). Some researchers have suggested that this canopy (composed of a connective tissue core covered by epithelium) creates a ventilatory dead space (Cooke, 1980) that protects developing lamellae [new lamellae are added at the base of the filament near the gill arch (Acrivo, 1935b)]. However, the canopy does not bind to the lamellae and thus there is sufficient space for water to enter and perfuse the interlamellar spaces. Therefore, while the branchial canopy likely protects the gill lamellae closest to the gill arch from bouts of high inertial water flow and mechanical damage (as indicated by a longer canopy near the cerato-epibranchial joint where inertial flow is likely strongest), these lamellae are still likely irrigated with ventilatory flow as water follows a path from high to low pressure. [Note: Unfortunately, it is not always clear whether the lamellae beneath the branchial canopy are included in estimates of elasmobranch gill surface area. These lamellae are included in gill area estimates by Wegner et al. (2010b) and Wootton et al. (2015), and, based on the similarity of gill morphometric data collected for overlapping species, likely Emery and Szczepanski (1986).]

As water passes the gill arch and branchial canopy it subsequently turns to flow between the lamellae of the gill filaments, which, in most fishes, are described as being perpendicular to the long-axis of each filament (Fig. 3.1E and F). Interestingly, several studies have reported that the lamellae of various

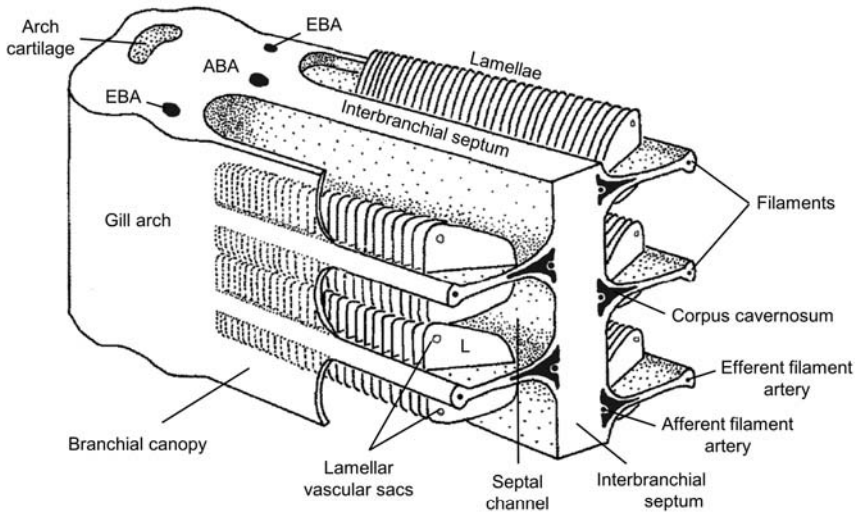

Figure 3.4. Detailed schematic of a cross-section through the elasmobranch gill arch and interbranchial septum showing the gill filaments and lamellae and associated features. ABA, afferent branchial artery; EBA, efferent branchial artery; L, lamella. Modified from Cooke (1980).

elasmobranch species are positioned at a slight angle to this long-axis with the leading lamellar edge angled toward the orobranchial cavity, thus slightly into the ventilatory stream (Fig. 3.4) and it has been suggested that this may help facilitate flow into the interlamellar spaces (Kempton, 1969; Wright, 1973; Cooke, 1980). However, the scope of this slight angle and its effects (if any) on water entry into the interlamellar spaces have not been quantified.

Elasmobranch lamellae are generally similar in shape to those of other fishes, typically with a semicircular or rectangular profile. However, elasmobranch lamellae differ in that they often possess distinct projections on the lateral leading edges that extend toward the orobranchial cavity (Fig. 3.5) (Cooke, 1980; Olson and Kent, 1980; Benz, 1984; De Vries and De Jager, 1984). Generally, these projections appear to be more pronounced and numerous in benthic elasmobranchs and to increase in number and size along the length of the filament (Fig. 3.5A) with up to five projections being reported on lamellae near the filament tip in some species (Cooke, 1980; Olson and Kent, 1980). Because lamellae on the filament tips are the oldest, Cooke (1980) suggested they might have an unknown function during early life stages. However, Olson and Kent (1980) observed a positive correlation of projections with body size in the spiny dogfish, *Squalus acanthias*, and the little skate, *Leucoraja erinacea*, and suggested that they might help direct flow into the interlamellar spaces. It seems likely that the increased size and

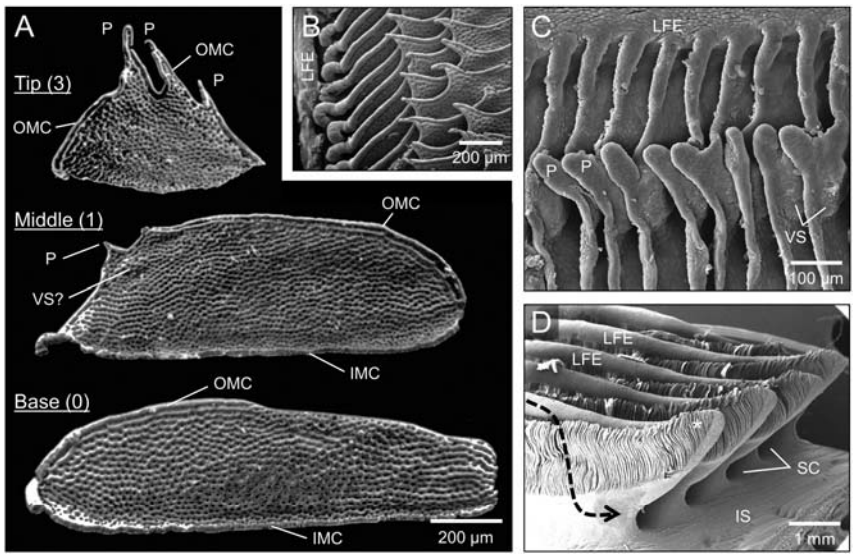

Figure 3.5. Scanning electron micrographs of elasmobranch lamellae showing their projections toward the orobranchial cavity. (A) Vascular casts of the lamellae of the smallfin gulper shark, *Centrophorus moluccensis*, revealing the variation in the shape and number of projections of lamellae sampled from the tip, middle, and base (top to bottom) of a representative filament. Numbers in parentheses indicate the number of projections. (B) Vascular casts of the lamellar projections of the spiny dogfish, *Squalus acanthias*. (C) Critical-point dried tissue showing the lamellar projections of the shortfin mako, *Isurus oxyrinchus* and closely associated vascular sacs. (D) Critical-point dried gill tissue of *I. oxyrinchus* showing the extension of lamellar projections above the leading edge of the filament tips (*). IMC, inner marginal channel; IS, interbranchial septum; LFE, leading filament edge; OMC, outer marginal channel; P, projection; SC, septal channel; VS, vascular sac. Water flow past the lamellae is from left to right in A and B, from top to bottom in C, and indicated by the dashed line in D. Modified from (A) Cooke (1980); (B) Olson and Kent (1980); (C and D) Wegner unpublished.

number of projections on lamellae near the filament tips would be useful in helping to bridge the gap between both adjacent filaments on the same arch and opposing filaments on opposing hemibranchs, thus minimizing the shunting of water flow past the filament tips without encountering the respiratory surfaces. Support for such a function is suggested by Fig. 3.5D, which shows lamellar projections at the filament tips in *I. oxyrinchus* extending above the rest of the filament.

In addition to a function in promoting more effective flow for gas exchange, there is also some suggestion that lamellar projections may help to promote lamellar stability. Vascular casting of the gill lamellae has shown the projections are perfused by a generally well-defined outer marginal

blood channel (Fig. 3.5A and B), which often has a constricted diameter near the apex of the projections (Olson and Kent, 1980). The added length of the outer marginal channel associated with traveling along several projections as well as the restricted diameter at key locations could serve to increase blood flow resistance, thus creating a hydrostatic skeleton to increase lamellar stiffness. In addition, a thick layer of collagen surrounding the outer marginal channel has been reported in the small-spotted catshark, *Scyliorhinus canicula*, and likely provides additional support to the free lamellar edge (Wright, 1973). In pelagic sharks such as *I. oxyrinchus* and the blue shark, *Prionace glauca*, these projections on the water-entry edge of the lamellae are often more subtle, but are associated with a thicker epithelium that has been suggested as a means to increase lamellar rigidity for ram ventilation (Wegner et al., 2010b).

In close proximity to the projections on the leading edge of the lamellae, at least some species have button-like bulges on either side of the lamellar surface that are aligned to abut bulges of adjacent lamellae (Figs 3.5C and 3.6). For *S. acanthias*, these bulges are described as being epithelial outgrowths (i.e., a thickening of the lamellar epithelium) (De Vries and De Jager, 1984), but in *I. oxyrinchus* and *P. glauca*, they result primarily from an increase in the diameter of the lamellar blood lumen (Fig. 3.6) and have been thus termed "vascular sacs" (Wegner et al., 2010b). Whether primarily epithelial or vascular in composition, the location of these bulges near the water-entry edge of the lamellae (Figs 3.4, 3.5C, and 3.6A) and a positive correlation of their abundance with lamellar size (Wegner, unpublished) suggests a function in ensuring lamellar stability and spacing (De Vries and De Jager, 1984; Wegner et al., 2010b). The vascular nature of these bulges in *I. oxyrinchus* and *P. glauca* suggests that vasoactive agents and changes in blood perfusion pressure could potentially influence sac size thereby modulating both lamellar rigidity and possibly the volume and speed of water passing through the interlamellar channels (Wegner et al., 2010b). Specifically, during bouts of increased activity, an increase in cardiac output and vasodilation could potentially distend the sacs thereby further stabilizing the lamellae and slowing a potentially fast and more forceful ventilatory stream. It is generally unknown if such epithelial or vascular bulges are species specific or a common elasmobranch feature simply not recognized or reported in many past studies. In addition to the species mentioned above, vascular sacs occur in all three thresher shark species (genus *Alopias*) (Wegner and Wootton, unpublished data), and a vascular sac appears present in the lamellar cast from a smallfin gulper shark, *Centrophorus moluccensis* from Cooke (1980) shown in Fig. 3.5A. In addition, Hughes et al. (1986) reported the presence of lamellar epithelial "thickened areas" for the nursehound, *Scyliorhinus stellaris*.

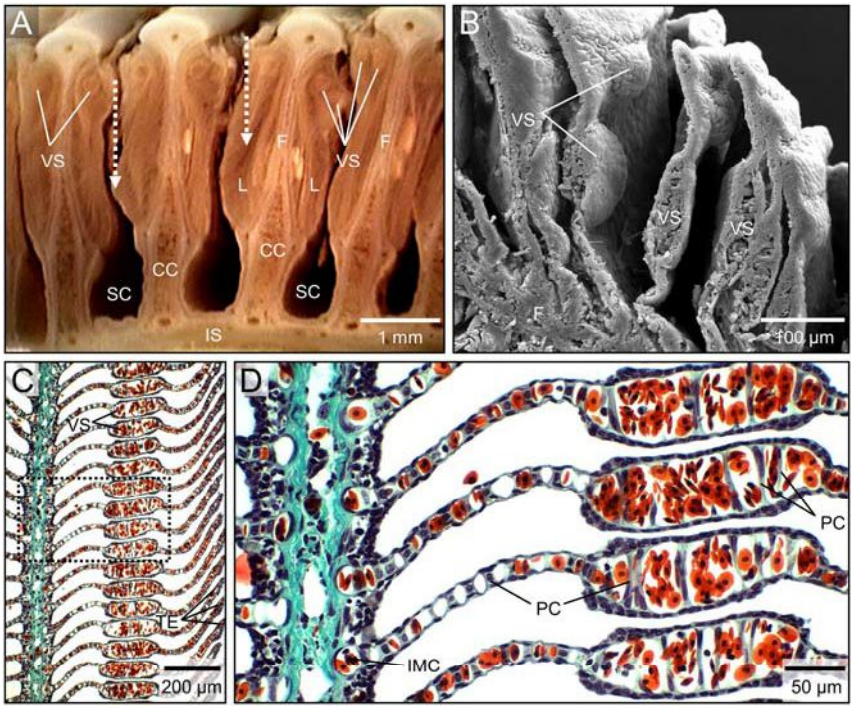

Figure 3.6. Micrographs of vascular sacs on the lamellae of the shortfin mako, *Isurus oxyrinchus*. (A) Section through four adjacent gill filaments showing one to two vascular sacs on each lamella near the leading (water-entry) edge. (B) Scanning electron micrograph of a longitudinal section through the gill filament showing the lamellar vascular sacs. (C) Light microscope image of a longitudinal filament section showing the proximity of vascular sacs from adjacent lamellae and the increased thickness of the lamellar epithelium near the outer marginal edge. (D) Magnified image of dotted box in (C) showing the details of the lamellar vascular sacs filled with red blood cells and supported by large pillar cells. Water flow is indicated by the dotted arrow in (A) and is into the page in (B–D). CC, corpus cavernosum; F, filament body; IMC, inner marginal channel; IS, interbranchial septum; L, lamella; PC, pillar cell; SC, septal channel; TE, thick epithelium; VS, vascular sac. From Wegner et al. (2010b).

5.2. Gill Vasculature

As with other fishes, the elasmobranch gill circulation has two main components or pathways: the respiratory vasculature (also referred to as the arterioarterial vasculature) and the nonrespiratory vasculature (also called the arteriovenous vasculature). The former provides blood to the respiratory lamellae for gas exchange and then proceeds to the systemic circulation for oxygen delivery to the tissues. The latter is a complex network that originates from the respiratory circulation and appears to have both

nutritive and lymphatic-like drainage functions and serves most of the filament epithelium involved in ion and pH balance (Laurent, 1984; Butler, 1999; Olson, 2002). Several studies using microvascular casting and histological techniques have allowed for a detailed understanding of both components for a variety of elasmobranchs ranging from rays (Donald, 1989; Sherman and Spieler, 1998; Basten et al., 2011) and skates (Dunel and Laurent, 1980; Olson and Kent, 1980; Laurent, 1984) to benthic (Kempton, 1969; Wright, 1973; Cooke, 1980; Dunel and Laurent, 1980; Olson and Kent, 1980; De Vries and De Jager, 1984; Laurent, 1984; Metcalfe and Butler, 1986) and pelagic sharks (Wegner et al., 2010b). Despite the use of different nomenclatures by various researchers to describe like structures (Laurent, 1984), the elasmobranch gill vasculature is largely conserved between species. A schematic overview of both the respiratory and nonrespiratory circulation of the gill filament is given in Fig. 3.7 in comparison to scanning electron microscopy images of a vascular cast filament for *I. oxyrinchus* (Fig. 3.8) and *S. acanthias* (Fig. 3.9A).

5.2.1. Respiratory Vasculature

Deoxygenated blood from the ventral aorta enters each gill arch through an afferent branchial artery that provides blood to the gill filaments via afferent distributing arteries (Figs 3.7 and 3.9A–C). Each distributing artery usually runs through the interbranchial septum for approximately one-third (range one-fifth to up to two-thirds) the length of the filaments to supply blood to one to four afferent filament arteries. Each afferent filament artery has two sections, a recurrent branch distributing blood to the basal section of each filament (closest to the arch), while a distal branch supplies the blood toward the filament tip. The recurrent and distal sections of each filament artery open at regular intervals to an extensive cavernous body (Figs 3.7, 3.8B and C, and 3.9A), with numerous collagen and elastic fiber-based trabeculae extending across its lumen, called the corpus cavernosum.

The corpus cavernosum extends medially from the afferent filament artery into the filament body (Figs 3.7–3.9) where it generally occupies the position of the cartilaginous filament rod in the filaments of most bony fishes (Figs 3.1F, 3.4, and 3.6A); filament rods are not found in elasmobranchs. While some have suggested the corpus cavernosum plays a role in the hemolysis of aging erythrocytes (Acrivo, 1935a) and may also function as a pulse-smoothing capacitance vessel prior to blood entry into the thin-walled lamellae (Wright, 1973; De Vries and De Jager, 1984), these views have not been substantiated (Metcalfe and Butler, 1986; Butler, 1999), and it is now generally accepted that its main function is as a hydrostatic skeleton that provides rigidity to the gill filaments. Direct evidence for this was provided by De Vries and De Jager (1984) who artificially applied

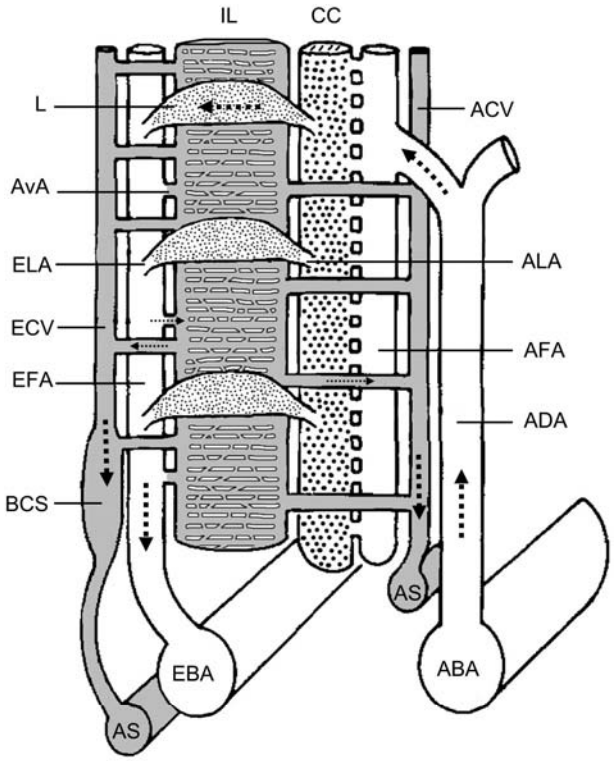

Figure 3.7. Schematic of the filament respiratory (white) and nonrespiratory (gray) circulation for a generalized elasmobranch. Dotted arrows indicate the direction of blood flow. ABA, afferent branchial artery; ACV, afferent companion vessel; ADA, afferent distributing artery; AFA, afferent filament artery; ALA, afferent lamellar arteriole; AS, arch sinus; AvA, arteriovenous anastomose; BCS, branchial canopy sinus; CC, corpus cavernosum; EBA, efferent branchial artery; ECV, efferent companion vessel; EFA, efferent filament artery; ELA, efferent lamellar arteriole; IL, interlamellar vessels; L, lamella. Modified from Donald (1989).

physiological blood pressures to the corpus cavernosum *in situ* and observed the erection of the filament tips away from the interbranchial septum to contact filament tips of the opposing hemibranch (the position normally observed in live animals).

In many species the corpus cavernosum also extends laterally into the septal tissues on either side of the afferent filament artery (Figs 3.8B and 3.9A and C). These lateral extensions, which may serve as anchor points for the filament bound portion of the corpus cavernosum, are relatively short near the base of the filaments, but become much more pronounced near the filament tips where septal cavernosa from adjacent filaments often

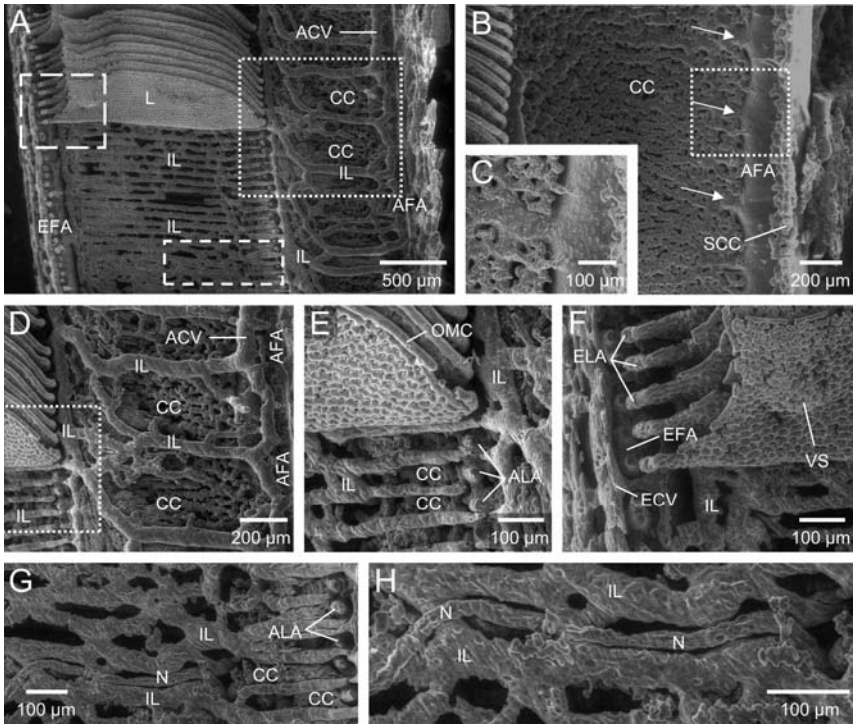

Figure 3.8. Scanning electron micrographs of vascular casts of the filament circulation from a shortfin mako, *Isurus oxyrinchus*. (A) Synoptic view of the gill filament circulation in the same orientation as that depicted graphically in Fig. 3.7. (B) Enlarged view of dotted box in (A) (upper right) with the interlamellar circulation removed to show the corpus cavernosum and its connections to the afferent filament artery (delineated by arrows). Also note the presence of the septal corpus cavernosum extending out of the page. (C) Magnified image of box in (B) showing both large and small connections of the afferent filament artery with the corpus cavernosum. (D) Enlarged image of dotted box in (A) (upper right) with the interlamellar circulation still intact. (E) Magnified image of dotted box in (D) showing the afferent lamellar arterioles leaving the corpus cavernosum and the interlamellar circulation running between the arterioles and underneath the lamellae. (F) Enlarged view of box in (A) (long dashes, upper left) showing the connection of the efferent lamellar arterioles to the efferent filament artery and the cast of a vascular sac on the efferent edge of a lamella. (G) Magnified image of box in (A) (short dashes, bottom middle) showing a nutrient vessel intertwined with the interlamellar circulation. (H) Enlarged view of (G). Water flow is from left to right in all images. ACV, afferent companion vessel; AFA, afferent filament artery; ALA, afferent lamellar arteriole; CC, corpus cavernosum; ECV, efferent companion vessel; EFA, efferent filament artery; ELA, efferent lamellar arteriole; L, lamella; IL, interlamellar vessel; OMC, outer marginal channel; SCC, septal corpus cavernosum; N, nutrient vessel; VS, vascular sac. Modified from Wegner et al. (2010b).

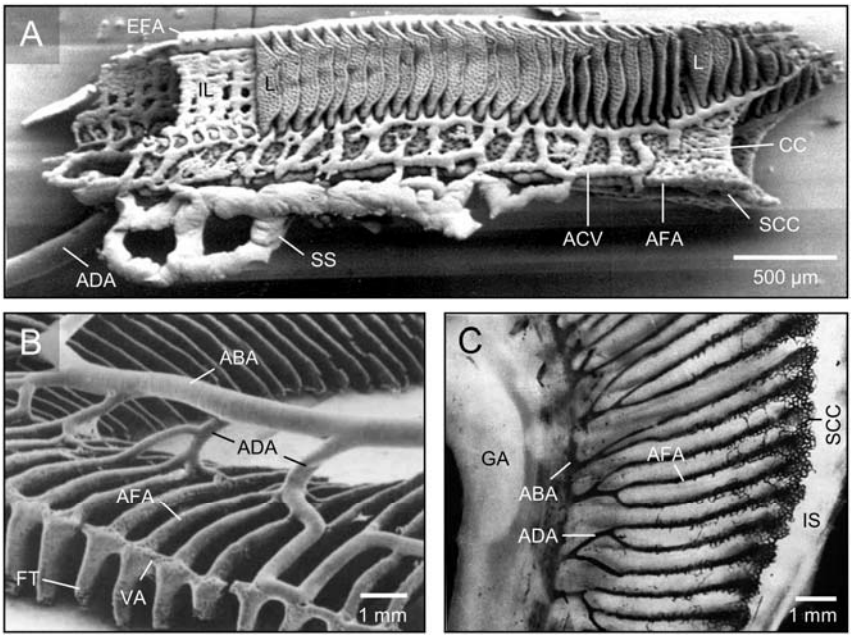

Figure 3.9. Vasculature of the elasmobranch gill. (A) Scanning electron micrograph of a vascular cast gill filament from the spiny dogfish, *Squalus acanthias*. (B) Scanning electron micrograph of a cast of the first gill arch of the western shovelnose stingaree, *Trygonoptera mucosa*, showing the afferent circulation providing blood to the gill filaments. Note the presence of the vascular cascade connecting adjacent afferent filament arteries near the filament tips. (C) Light micrograph of an Indian ink injected gill arch of the small-spotted catshark, *Scyliorhinus canicula*, with the top hemibranch removed to show the afferent circulation of the underlying hemibranch. Note the interconnections of the septal corpus cavernosum (SCC) of adjacent afferent filament arteries near the filament tips. Other abbreviations: ABA; afferent branchial artery; ACV, afferent companion vessel; ADA, afferent distributing artery; AFA, afferent filament artery; CC, corpus cavernosum; EFA, efferent filament artery; FT, filament tip; GA, gill arch; IL, interlamellar vessels; IS; interbranchial septum; L, lamella; SS, septal sinus; VA, vascular arcade. Modified from (A) Olson and Kent (1980); (B) Donald (1989); (C) Wright (1973).

anastomose together (Fig. 3.9C). During exercise, increased blood pressure may thus not only increase the rigidity of the gill filaments, but may also increase the stiffness of the interbranchial septum. Interestingly, urolophid stingrays lack the septal portion of the corpus cavernosum, which appears to be replaced by or perhaps reduced to a single vessel-like "vascular arcade," which connects the afferent filament arteries near the filament tips (Fig. 3.9B) (Donald, 1989; Sherman and Spieler, 1998; Basten et al., 2011). The lack of septal cavernosa in urolophids may correlate with their

general inactivity, and hence a reduced need for a stiff interbranchial septum or septal-anchored filament cavernosa.

Arising from the filament portion of the corpus cavernosum are short lamellar arterioles that provide blood to the respiratory lamellae (Figs 3.7 and 3.8E). Like most other fishes, blood flow through elasmobranch lamellae is thought to be sheet-like (Farrell et al., 1980), although the placement of the pillar cells running across the lumen often appears to delineate rough channels or preferred routes (Figs 3.5A and 3.8E). The outer marginal channel is particularly well defined, and, as mentioned previously, may have a hydrostatic functional capacity. In addition, one or more inner marginal channels are typically embedded within the body of the filament (Figs 3.1G and H, and 3.6D). Following gas exchange, oxygenated blood exits the lamellae via efferent lamellar arterioles that empty into an efferent filament artery (Figs 3.7, 3.8F, and 3.9A) that runs along the length of each filament and brings blood back to the gill arch (Fig. 3.7). Blood from the efferent filament arteries of each hemibranch is collected by a separate efferent branchial artery (thus with the exception of the first gill arch, which only has a posterior-facing hemibranch, there are two efferent branchial arteries per arch), from which it proceeds to the systemic circulation.

5.2.2. Nonrespiratory Vasculature

Stemming from the respiratory circulation is the nonrespiratory or arteriovenous vasculature. The nonrespiratory vasculature is often subdivided into two parts: the interlamellar circulation (also referred to as the lymphatic-venous circulation) and the nutrient circulation, although this division is still equivocal (Laurent, 1984; Olson, 2002). The complex network of interlamellar vessels within the filament body (often termed the central venous sinus) comprise a low-pressure system that generally runs parallel to the inner margins of the lamellae (Figs 3.7, 3.8A, D–H, and 3.9A) and is thought to be closely associated with the filament epithelium where MRCs are present in high abundance (Olson and Kent, 1980; Laurent, 1984; Olson, 2002; Wilson and Laurent, 2002; Evans et al., 2005). Depending on the species, these vessels appear to receive blood from a combination of small anastomoses with the efferent filament artery (Fig. 3.7), efferent lamellar arterioles, and or corpus cavernosum. Intermingled with, but largely separate from the interlamellar or central venous sinus vessels are nutrient vessels that course through the filaments and interbranchial septa (Fig. 3.8G and H). The nutrient vessels appear to originate from the efferent filament and branchial arteries and drain into the interlamellar circulation. Within the filament, the interlamellar and some nutrient vessels drain into afferent and efferent companion vessels that run parallel to the afferent and efferent filament arteries (Figs 3.7, 3.8D and F, and 3.9A) (Note: afferent

and efferent used here refer solely to their location in proximity to the afferent and efferent filament arteries and not to a function associated with gas exchange). Along their course toward the gill arch the afferent companion vessels often connect and drain into large sinuses within the interbranchial septum (Fig. 3.9A), while the efferent companion vessels may connect with sinuses within the branchial canopy (Fig. 3.7). Ultimately this low-pressure system empties into septal and gill arch sinuses that drain dorsally into the anterior cardinal sinus and ventrally into the inferior jugular sinus (De Vries and De Jager, 1984; Butler, 1999).

5.2.3. Gill Vasculature and Blood Shunting

Early physiological studies on elasmobranch respiratory function showed highly variable gill O_2 utilization and correlating variable dorsal aortic PO_2 levels (e.g., Lenfant and Johansen, 1966; Piiper and Schumann, 1967; Grigg and Read, 1970), and Piiper and Schumann (1967) and others suggested this might be associated with the shunting of blood around the respiratory surfaces of the gills through the nonrespiratory circulation. Such shunting would indicate the ability of elasmobranchs to modulate blood flow through the gills to meet aerobic demands under different physiological conditions (e.g., exercise vs. rest), the benefit of which would allow for a decreased perfusion of the thin respiratory surfaces, and hence a decrease in passive ion movement between the blood and water (=reduced ionic regulatory costs) during bouts of relative inactivity. As a result, most of the early studies on elasmobranch gill vasculature examined the potential for nonrespiratory shunts of blood to bypass the respiratory exchange surfaces. Although the nonrespiratory interlamellar circulation in several species anastomoses with both the afferent and efferent respiratory vasculature, it is generally considered a distensible venolymphatic system, which is generally free of red blood cells and operates at pressures well below that of both the afferent and efferent filament arteries and is thus unable to serve as a physiological bypass.

Rather than vascular shunts, it is now generally thought that ionic regulatory costs can be minimized during rest by regional changes in the distribution or perfusion of blood through the respiratory surfaces with large regions of the gills being essentially shutdown during rest and recruited during exercise. Regional changes in gill blood flow has been shown for several elasmobranchs (e.g., Satchell et al., 1970; Cameron et al., 1971) and is likely achieved through regional differences in vascular resistance, the use of sphincters (which are present at numerous locations throughout the gill vasculature), and changes in blood perfusion pressures induced by varying levels of cardiac output with activity (e.g., at reduced cardiac outputs, fewer lamellae would be perfused with blood). Variable oxygen extraction

efficiencies and dorsal aortic PO_2 values could also result from changes in ventilation – perfusion matching (Piiper and Scheid, 1984; Butler and Metcalfe, 1988; Bhargava et al., 1992) with the coordination in timing of the pulsatile blood and ventilatory flow increasing O_2 uptake, and a mismatch decreasing utilization. However, such mismatches are unlikely to mitigate ionic regulatory costs and models suggest that in sedentary species such as *S. stellaris*, a mismatch in ventilation-perfusion timing has little effect on gas exchange (Malte, 1992).

An interesting exception to the lack of true vascular shunts may be present in urolophid rays, in which some afferent filament arteries appear to be directly connected to their corresponding efferent filament artery at the filament tip (Donald, 1989; Sherman and Spieler, 1998). The extent to which blood flows through the filament tip and bypasses the respiratory exchange surfaces (and the extent to which this can be controlled) remains unknown and deserves additional study. For rays, such a bypass would be particularly useful as they are often at rest on the substrate and thus would only occasionally require additional capacity for increased O_2 uptake.

5.3. The Gill Epithelium

The gill epithelium is heavily involved in several life-sustaining processes. It provides both a barrier and a means of transport for molecules between the internal and external environments and is thus vital for homeostasis. Elasmobranch lamellar and filament epithelia are similar to those of other fishes and detailed comparative accounts can be found in reviews by Laurent (1984), Wilson and Laurent (2002), and Evans et al. (2005). The lamellar epithelium is typically composed of one to three layers of epithelial cells, with polygonal squamous pavement cells lining most of the apical (outer) surface (Figs 3.10 and 3.11). The surface of these cells typically have finger-like microvilli or microridges that are thought to help anchor a mucous layer that provides protection from bacteria and other foreign materials, reduces gill drag (Daniel, 1981), and likely decreases the permeability of the epithelium to certain ions and other molecules (Hill et al., 2004). Subsurface to the pavement cells typically lie undifferentiated epithelial cells distributed over a basement membrane (=basal lamina) that separates the epithelium from the lamellar vasculature. Epithelial cell nuclei are often positioned above the columns of pillar cells (Figs 3.6D and 3.10) which allows for decreased epithelial thickness over the blood channels where most gas exchange occurs. However, in benthic elasmobranchs (which typically have relatively low metabolic demands), specialized cells, namely MRCs (also called chloride cells due to their role in chloride excretion from the gills of marine teleosts) and goblet cells (=mucous cells) can also be found in the

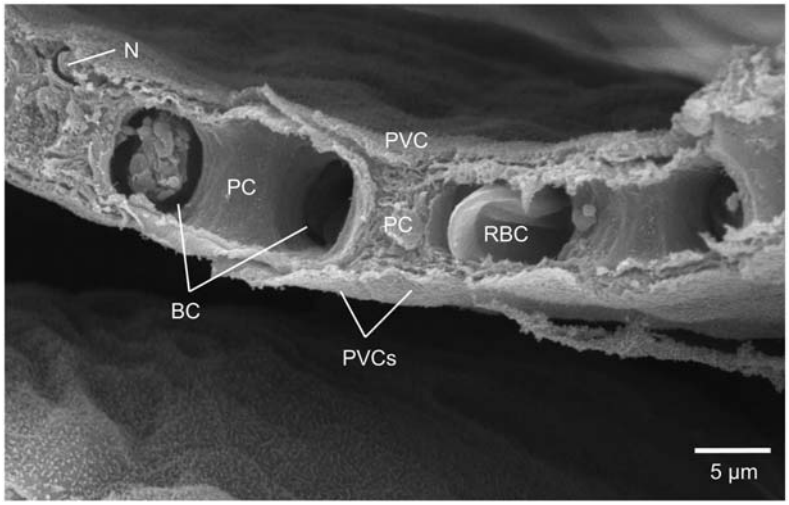

Figure 3.10. Cross-section through a lamella of the shortfin mako, *Isurus oxyrinchus*, showing the lamellar blood channels (BCs) formed by pillar cells (PCs) and the overlaying lamellar epithelium composed primarily of thin pavement cells (PVCs). Note the location of a pavement cell epithelial nucleus (N) above the pillar cell column so as to limit the diffusion distance immediately above the BCs. Below the cross-sectioned lamella is the epithelial surface of the adjacent lamella showing the microvilli and microridges characteristic of fish gill epithelia. RBC, red blood cell.

lamellar epithelium (Hughes and Wright, 1970; Wright, 1973; Sala et al., 1987; Duncan et al., 2010). Because their large size increases diffusion distances, these specialized cells are usually more abundant in the filament epithelium, especially in more active species that require short diffusion distances (Wegner et al., 2010b).

The filament epithelium is generally similar to that of the lamellae although it is typically much thicker (three or more layers of cells) and contains regionally higher concentrations of MRCs and goblet cells (Fig. 3.11). As in teleosts, MRCs appear to be most abundant in the interlamellar filament epithelium where they overlay and likely interact with the interlamellar circulation (Wright, 1973; Olson and Kent, 1980; Laurent, 1984; Wilson and Laurent, 2002) and are also in close approximation to the inner marginal channels of the lamellae. Goblet cells can be found throughout the filament epithelium and are often highly concentrated on both the leading and trailing edges of the filament, as well as the interlamellar spaces.

MRCs in elasmobranchs are thought to be used primarily in salt uptake and acid-base balance (similar in function to those of freshwater teleosts), rather than the primary marine teleost function in Na^+ and Cl^- excretion

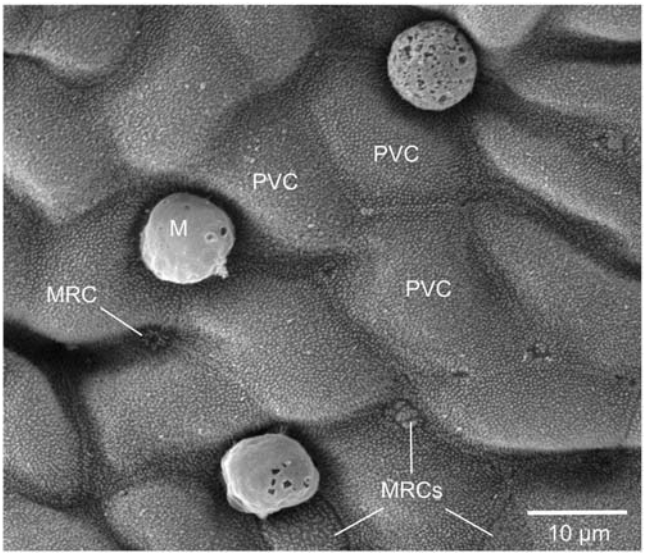

Figure 3.11. Scanning electron micrograph of the filament epithelial surface along the septal channel of the common thresher shark, *Alopias vulpinus*, showing pavement cells (PVCs), mucus (M) emerging from goblet cell pores, and the apical surface of mitochondrion-rich cells (MRCs) emerging between some pavement cells. Note the difference in the microvillar pattern of pavement and MRCs.

(Wilson et al., 1997; Piermarini and Evans, 2001; Evans et al., 2004; Tresguerres et al., 2006; Roa et al., 2014; Wright and Wood, 2015). Thus, unlike marine teleosts, elasmobranch MRCs are usually found singly with nonleaky, tight junctions between neighboring pavement cells (Wilson et al., 1997, 2002), which differs from the configuration observed for marine bony fishes in which MRCs are usually accompanied by accessory cells with leaky tight junctions that create a paracellular route for Na^+ efflux (Laurent, 1984; Wilson and Laurent, 2002; Evans et al., 2005). Superficially, elasmobranch MRCs are generally similar to those of teleosts with high mitochondrial densities, a basally located nucleus, and a densely packed sub-apical tubulovesicular system (Fig. 3.12). The apical surface of MRCs can be highly variable, ranging from deep invaginations to convex crests (Laurent, 1984; Wilson and Laurent, 2002; Wilson et al., 2002), but appears to always be covered with microvilli that are typically longer or have a different pattern than those of the surrounding pavement cells (Hughes and Wright, 1970; Wilson et al., 2002; Evans et al., 2005) (Fig. 3.11). While the function of these microvilli is still largely unclear, there does appear to be a positive correlation between microvillar size with MRC activity, as the microvilli tend to become

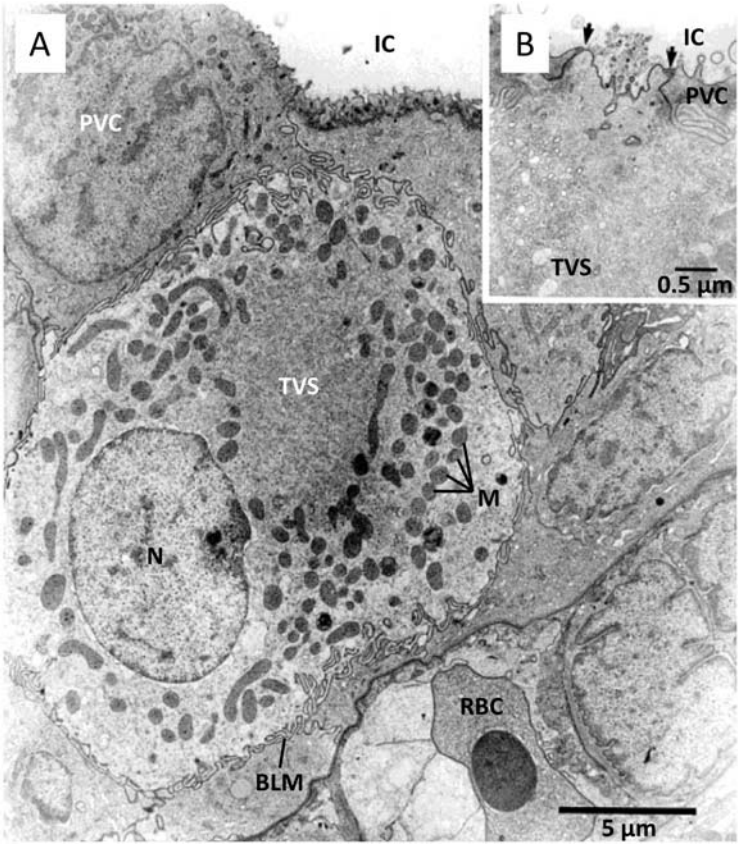

Figure 3.12. (A) Transmission electron micrograph (TEM) section of a mitochondrion-rich cell (MRC) from the interlamellar filament epithelium of the spiny dogfish, *Squalus acanthias*, showing the basally located nucleus (N), supranuclear tubulovesicular system (TVS), numerous mitochondria (M), and the basolateral plasma membrane (BLM) with extensive infoldings. The MRC is in close proximity to both the interlamellar water channel (IC) and gill vasculature (bottom right) containing red blood cells (RBCs). (B) TEM section of an MRC showing the apical surface and the nonleaky tight junctions (arrowheads) between the MRC and adjacent pavement cells (PVCs). Modified from Wilson et al. (1997).

larger and or thicker with exposure to divalent ions (e.g., Zn^{2+}) or freshwater (Crespo, 1982). Elasmobranch MRCs lack the tortuous basolateral tubular system of marine teleosts (Laurent, 1984; Sala et al., 1987; Wilson et al., 1997), but have extensive infoldings of the basolateral membrane (Fig. 3.12) that are the sites of Na^+-K^+-ATPase expression in some MRCs, while other MRCs express vacuolar-proton ATPase (V-H^+-ATPase) in the cytoplasm that inserts into the basolateral membrane upon blood alkalosis (Fig. 3.13). Cells

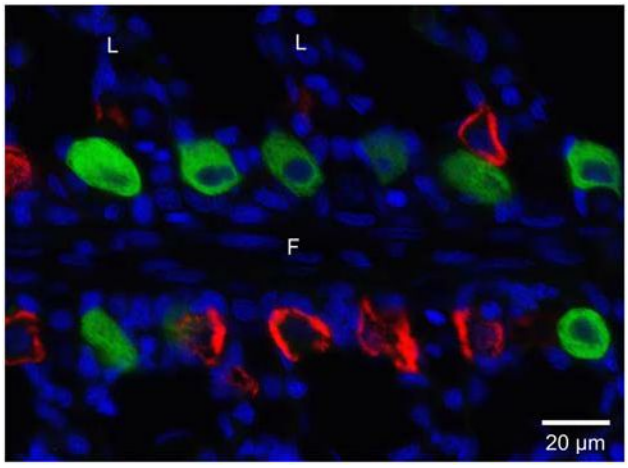

Figure 3.13. Immunofluorescent-stained longitudinal section through a gill filament of the leopard shark, *Triakis semifasciata*, showing the presence of two mitochondrion-rich cell (MRC) subtypes in the interlamellar filament epithelium: MRCs with Na^+-K^+-ATPase (red) and MRCs with V-H^+-ATPase (green). Cell nuclei are stained blue. L, lamellae; F, filament body. Image courtesy of J. Roa and M. Tresguerres.

with Na^+-K^+-ATPase expression are specialized for H^+ excretion (in exchange for Na^+ uptake), while those with V-H^+-ATPase excrete HCO_3^- (in exchange for Cl^-) (Piermarini and Evans, 2001; Evans et al., 2004, 2005; Tresguerres et al., 2006; Roa et al., 2014).

In addition to MR and goblet cells, the elasmobranch filament epithelium also contains neuroepithelial cells (Laurent, 1984), which are found deep within the epithelium and are thought to play a role in oxygen sensing and the regulation of blood flow (Sundin and Nilsson, 2002). Finally, large flask-shaped cells with a narrow apical region, abundant mitochondria, and numerous vesicles have been documented in the filament epithelium of some elasmobranchs, but their function is unknown (Wright, 1973; Wilson et al., 2002).

6. DIVERSITY IN ELASMOBRANCH GILL DIMENSIONS AND MORPHOLOGY

The first several sections of this chapter have focused primarily on common structural features of the elasmobranch gill. However, as in bony fishes, elasmobranch gill morphology varies in relation to habitat and life history. While elasmobranchs are not nearly as diverse as teleosts, they have

nonetheless filled a number of different niches resulting in varied body plans or ecomorphotypes (Compagno, 1990), ranging from freshwater stingrays to the highly streamlined and regionally endothermic sharks of the open ocean. This section focuses on functional differences within the elasmobranch gill and its specialization for increased oxygen uptake, enhanced osmoregulatory function, and adaptations associated with feeding.

6.1. Gill Arches

Perhaps one of the most obvious examples of diversity in elasmobranch gill morphology is variation in the number of gill bearing arches. Most elasmobranchs have five gill arches containing nine hemibranchs (one hemibranch on the hyoid arch followed by four holobranchs) on either side of the orobranchial cavity (Fig. 3.1B). However, well known are the Hexanchiformes, which include the frill shark, *Chlamydoselachus anguineus*, and the sixgill sharks (*Hexanchus* spp.) which have six branchial arches (one hemibranch and five holobranchs) on either side of the orobranchial chamber, as well as the sevengill sharks (*Heptranchias, Notorynchus*) which have seven (one hemibranch and six holobranchs) (Fig. 3.14). While it has been tempting for some evolutionary biologists to draw the parallel between the seven paired gill pouches of lampreys and the seven arch pairs of some Hexanchiformes (which in some previous phylogenies were positioned near the base of the elasmobranch tree), there is little evidence to support that seven (or six) gill arches is the basal elasmobranch character state (especially considering the first two arches in gnathostomes have moved forward to form and support the jaws). Examination of the "extra" gill arches points to their independent evolution in *Chlamydoselachus* and *Hexanchus* (thus challenging the monophyly of the hexanchoids) with the additional independent evolution of an extra arch pair in the sevengill sharks (Shirai, 1992). In addition to the Hexanchiformes, a single species of saw shark, the sixgill sawshark, *Pliotrema warren* (Order Pristiophoriformes), and at least one ray species, the sixgill stingray *Hexatrygon bickelii* (Order Myliobatiformes) have six gill arch pairs. Thus it appears that the evolution of additional gill arches has occurred multiple times within elasmobranchs, and it seems reasonable that this characteristic may be related to the deep, and presumably low-oxygen habitats that these species tend to inhabit (with the notable exception of *Notorynchus*, which is a generally shallow water, coastal species). However, measurements of gill surface area are needed to support this hypothesis.

Another interesting deviation from the normal elasmobranch branchial arch configuration occurs in the collared carpet sharks (Family Parascylliidae, Order Orectolobiformes). These sharks have five gill arch pairs

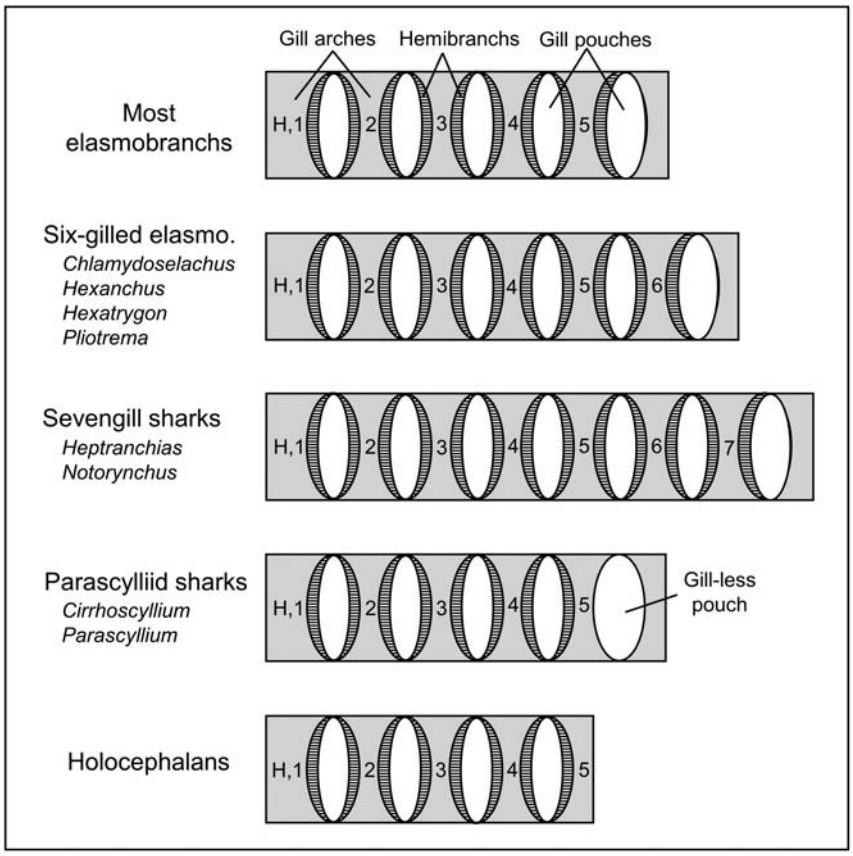

Figure 3.14. Simplified schematic showing the diversity in elasmobranch gill arch number and hemibranch configuration (also shown are the closely related holocephalans). H, hyoid arch (also referred to in this text as gill arch 1).

like most elasmobranch species, but lack filaments on the posterior side of the fifth arch (Goto et al., 2013). The fifth parabranchial cavity thus lacks any respiratory gill tissue (Fig. 3.14) and has a strikingly large gill slit [most gill slits tend to remain constant or decrease in height along the length of the shark (Dolce and Wilga, 2013)] that appears to be used to create extra force during suction feeding (Goto et al., 2013). As parascylliid sharks are coastal benthic species that inhabit well oxygenated waters and likely have low oxygen demands, the forfeit of this hemibranch appears to be an acceptable loss in order to enhance their ability for prey capture through suction feeding.

6.2. Gill Morphometrics

Even without gill specialization that includes the addition or loss of gill arches or hemibranchs, the size of the gills can vary widely among species, and while the gill is involved in multiple functions, such differences in gill morphometrics appear to correlate most directly with its function in gas exchange. The rate of oxygen uptake ($\dot{M}O_2$ in $mgO_2\ min^{-1}$) at the gill is directly related to both gill dimensions and dissolved oxygen levels within the environment as described by the Fick equation:

$$\dot{M}O_2 = (K \cdot A \cdot \Delta P_{O_2})/t \tag{3.1}$$

where K is the diffusion or Krogh coefficient through a specific material (e.g., the gill epithelium, mgO_2 μm cm^{-2} $mmHg^{-1}$ min^{-1}), A is the respiratory surface area of the gills (usually reported as the total bilateral surface area of all the lamellae in the gills in cm^2), ΔP_{O_2} is the mean difference in the partial pressure of oxygen between the water and the blood (mmHg), and t is the diffusion distance (μm).

According to Eq. (3.1), increases in gill surface area (A) or a decrease in diffusion distance (t) will augment oxygen uptake. If ΔP_{O_2} is low due to low levels of environmental oxygen, an increase in A or decrease in t are needed to maintain the same level of oxygen uptake. As a result, gill surface area and gill diffusion distances correlate with both oxygen demands and the dissolved oxygen levels of the environment. Fig. 3.15 shows the gill surface areas for all elasmobranchs determined to date, with highly-active species having larger gill surface areas than those of less-active, benthic species. Particularly large are the gill surface areas of the lamnid sharks (Family Lamnidae) and the thresher sharks (Family Alopiidae), which are highly active predators, many of which are able to increase aerobic performance through regional endothermy (Bernal et al., 2012).

The relationship between resting metabolic rate and gill surface area for the few elasmobranchs for which accurate data are available for both variables is shown in Table 3.1. While some caution should be used when extrapolating regression equations for gill surface area and metabolic rate to a common mass for interspecific comparisons (in this case 1 kg, which is not a realistic size for some species), the metabolic rate to gill surface area ratio is strikingly similar between species of varying activity levels, indicating their close correlation. However, considering that functional gill area can be reduced during rest (e.g., through changes in blood perfusion, see Section 5.2.3), it seems likely that gill area may correlate even more tightly with maximum sustainable metabolic rate, and this may help explain some of the variation in Table 3.1. Hence the relatively small gill surface area relative to resting metabolic rate in the marbled electric ray,

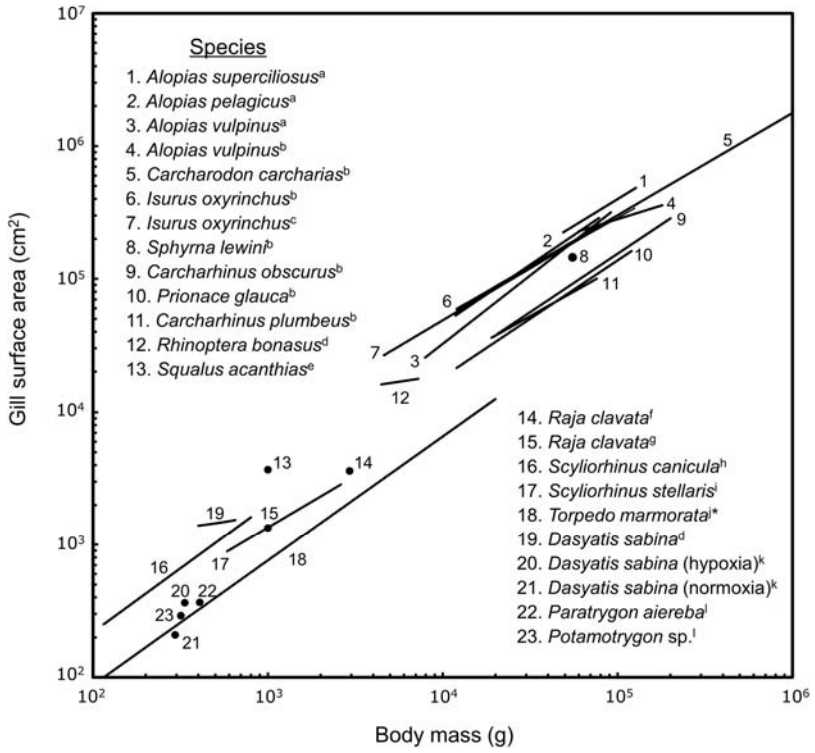

Figure 3.15. Relationship of gill surface area to body mass for all known elasmobranchs studied to date. Note: Gill areas estimated for the megamouth shark, *Megachasma pelagios*, and shortfin mako, *Isurus oxyrinchus*, by Oikawa and Kanda (1997) are not included in the present figure as they were shown to be inaccurate (Wegner et al., 2010b). *Regression line for *Torpedo marmorata* includes five specimens of the electric ray, *T. nobiliana*. The single data point for the scalloped hammerhead, *Sphyrna lewini*, is the mean of three individuals estimated from a gill-area-to-body-mass graph from Emery and Szczepanski (1986). Sources: Wootton et al. (2015)[a], Emery and Szczepanski (1986)[b], Wegner et al. (2010b)[c], Grim et al. (2012)[d], Boylan and Lockwood (1962)[e], Hughes and Morgan (1973)[f], Hughes (1977)[g], Hughes (1972)[h], Hughes et al. (1986)[i], Hughes (1978)[j], Dabruzzi and Bennett (2013)[k], Duncan et al. (2011)[l].

Torpedo marmorata (=high ratio of resting metabolic rate to gill area compared to other species in Table 3.1) may indicate that this species is not able to increase its oxygen uptake much above that at rest. For a species such a *T. marmorata* with low activity levels this may not be problematic and should reduce costs associated with osmoregulation. Unfortunately, comparing maximum metabolic rate to gill surface area is difficult due to the challenge of conditioning sharks and rays to swim steadily in swim tunnel respirometers at maximum sustainable speeds.

Table 3.1
Relationship between resting metabolic rate (RMR) and gill surface area for five elasmobranchs

Common name	Species names	RMR (mgO_2 kg^{-1} h^{-1})	Gill area for 1 kg fish (cm^2)	RMR/area (mgO_2 h^{-1} m^{-2})
Sandbar shark	*Carcharhinus plumbeus*	47.23[a]	4074[b]	115.93
Spiny dogfish	*Squalus acanthias*	52.64[c]	3700[d]	142.27
Shortfin mako	*Isurus oxyrinchus*	141.57[e]	9550[b]	148.24
Shortfin mako	*Isurus oxyrinchus*	141.57[e]	8038[f]	176.13
Small-spotted catshark	*Scyliorhinus canicula*	38.20[g]	2004[h]	190.62
Marbled electric ray	*Torpedo marmorata*	20.72[i]	759[i]	272.99

RMRs were adjusted to 15°C using a Q_{10} of 2 and to a body mass (M) of 1.0 kg using $M^{0.80}$ (unless species-specific scaling coefficients were known).

Metabolic studies lacking experimental temperature or body mass data or using data from animals that were surgically stressed (e.g., Piiper and Schumann, 1967) are not included.

Sources:
[a]Dowd et al. (2006).
[b]Emery and Szczepanski (1986).
[c]Brett and Blackburn (1978).
[d]Boylan and Lockwood (1962).
[e]Sepulveda et al. (2007).
[f]Wegner et al. (2010b).
[g]Sims (1996).
[h]Hughes (1972).
[i]Hughes (1978).

Missing from Table 3.1 is the incorporation of diffusion distance data, which according to Eq. (3.1) equally affects the rate of oxygen uptake. Diffusion distance data are difficult to incorporate into models of oxygen uptake as oxygen must travel through the interlamellar water, the lamellar epithelium, the blood, and into erythrocytes where it binds to hemoglobin. Thus, diffusion distances are tied to multiple measurements, as well as the hydrodynamics of the ventilatory stream and blood flow. Still, insight can be gained by examining the thickness of the water–blood barrier and thickness of the lamellae themselves (Table 3.2). These tend to be thin in active, pelagic sharks. For example, *I. oxyrinchus* has a water–blood barrier approximately an order of magnitude thinner than some benthic shark species.

6.3. Theory on Elasmobranch Gill Dimensions and Limits to Gill Diffusion Capacity

Gill surface area (A) is the product of a number of constituent dimensions:

$$A = L_{fil} \cdot 2n_{lam} \cdot A_{lam} \quad (3.2)$$

Table 3.2
Thickness of the water–blood barrier and lamellae reported for elasmobranchs of varying activity level and habitat

Common name	Species name	Water–blood barrier thickness (μm)	Lamellar thickness (μm)	Reference
Shortfin mako	*Isurus oxyrinchus*	1.15±0.22	11.38±1.61	Wegner et al. (2010b)
Bigeye thresher	*Alopias superciliosus*	1.60±0.08	12.50±2.59	Wootton et al. (2015)
Pelagic thresher	*Alopias pelagicus*	1.61±0.19	12.51±0.53	Wootton et al. (2015)
Blue shark	*Prionace glauca*	1.65±0.59	15.24±3.41	Wegner et al. (2010b)
Common thresher	*Alopias vulpinus*	2.55±0.27	14.29±0.94	Wootton et al. (2015)
Spotted skate	*Raja montagui*	4.85		Hughes and Wright (1970)
Thornback skate	*Raja clavata*	5.99		Hughes and Wright (1970)
Nursehound	*Scyliorhinus stellaris*	9.43±1.72	34.1	Hughes et al. (1986)
Nursehound	*Scyliorhinus stellaris*	9.62		Hughes and Wright (1970)
Tope	*Galeorhinus galeus*	9.87		Hughes and Wright (1970)
Spiny dogfish	*Squalus acanthias*	10.14		Hughes and Wright (1970)
Small-spotted catshark	*Scyliorhinus canicula*	11.27		Hughes and Wright (1970)

Note: The diffusion distance data compiled in this table clearly show a correlation with elasmobranch activity level. However, techniques for measuring and preparing samples can vary between studies, which can affect results and should thus be considered when making comparisons. For example, Hughes (1984) notes that the electromicrograph sections used for measurements in Hughes and Wright (1970) were not always cut and mounted exactly perpendicular to the lamellar surface, thus likely resulting in some overestimation of thickness. However, reexamined measurements for *S. stellaris* (Hughes et al., 1986) in which harmonic means of the water–blood barrier were calculated and values were corrected for the Holmes effect, slant, and shrinkage, were only about 2% different than the original estimates. Still additional and repeat studies of diffusion distances in the gills are warranted, especially in species for which a surprisingly thick water–blood barrier is reported. For example, micrographs in several studies (including those in Hughes and Wright, 1970) show water–blood barrier distances much shorter than the means reported in this table by Hughes and Wright (1970).

where L_{fil} is the total length of all the gill filaments, n_{lam} is the number of lamellae per unit length on one side of a filament (i.e., lamellar frequency, which is multiplied by two to account for lamellae on each side of the filament), and A_{lam} is the mean bilateral surface area of a lamella. Consequently, an increase in any of these dimensions results in a larger gill surface area.

While gill surface area correlates with metabolic demand, these componential dimensions (L_{fil}, n_{lam}, A_{lam}) are sculpted by various factors. Particularly important are hydrodynamic considerations that must be balanced to create optimal ventilatory-flow conditions in the interlamellar channels for gas exchange (Strother, 2013; Park et al., 2014). The velocity (and consequently residence time) of water in contact with the lamellae in the interlamellar channels is largely dependent on the resistance imposed by the gills. Resistance (R) through the interlamellar channels is described by the Hagen-Poiseuille equation for water flow between parallel plates. For a single interlamellar channel:

$$R = 12\mu l/d^3 h \tag{3.3}$$

and for all interlamellar channels in the gills:

$$R = 12\mu l(d + w)/d^3 h L_{fil} \tag{3.4}$$

where μ is the dynamic viscosity of the water, l is the length of the interlamellar channel, d is the diameter or width of the channel, w is the width or thickness of a lamella, and h is the lamellar height (dimensions shown in Fig. 3.16). According to this equation, an increase in lamellar

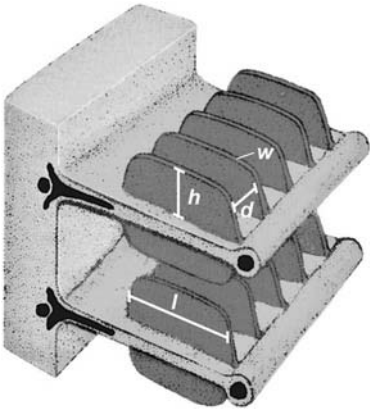

Figure 3.16. Schematic from Fig. 3.1 showing lamellar dimensions associated with Eqs (3.3) and (3.4). Variable abbreviations: d, diameter of interlamellar channel; h, lamellar height; l, lamellar length (=length of interlamellar channel); w, lamellar thickness.

length (l) or lamellar frequency (thus decreasing d) amplifies gill resistance (and consequently the energy required to ventilate the gills), while an increase to lamellar height (h) or the length of the gill filaments (L_{fil}), decreases gill resistance. Thus, from an energetic standpoint (i.e., minimizing increases to gill resistance), gill surface area is optimally increased through large (tall) lamellae and high total filament lengths (Hughes, 1966; Wegner, 2011).

In reality, certain fish groups appear to adhere to this optimal configuration to augment gill area, while others do not. For high-energy demand and ram-ventilating teleosts such as tunas (family Scombridae), gill surface area is increased through long gill filaments, but also through high lamellar frequencies, which decreases d and greatly amplifies gill resistance (Muir and Hughes, 1969; Wegner et al., 2010a). Wegner et al., (2010a) suggested the increase in resistance imposed by high lamellar frequencies might help slow the fast and forceful branchial stream produced by ram-ventilation to create more optimal conditions for efficient gas exchange. In contrast to high-performance teleosts, fast-swimming elasmobranchs (e.g., the lamnid sharks) do not have increased lamellar frequencies, but rather adhere to the theorized optimal configuration by increasing gill area through long filaments and large lamellae (Emery and Szczepanski, 1986; Wegner et al., 2010b). Because the septal channels contribute substantially to gill resistance (Wegner et al., 2012), high lamellar frequencies, which would further increase resistance, are likely precluded as a metric in elasmobranchs to increase gill surface area. Consequently and because increased filament length and large lamellae require additional space within the branchial chambers (high lamellar frequencies do not), total gill surface area is quickly constrained in fast swimming elasmobranchs by the dimensions of the branchial chambers and cranial streamlining. Thus in comparison to tunas (the zenith of teleost aerobic performance), lamnid sharks (the peak of elasmobranch performance) have one-half the lamellar frequency, which results in approximately one-half the total gill surface area, and likely limits elasmobranch aerobic capacity in comparison to teleosts (Wegner et al., 2010b, 2012).

In addition to apparent limits in gill surface area, gill diffusion distances in elasmobranchs are generally longer than those of teleost species that are similar in activity level and habitat. First, elasmobranch interlamellar channels are generally wider in order to compensate for the added resistance of the septal channels. Second, the water–blood barrier in elasmobranchs is generally thicker (Hughes and Wright, 1970; Wegner et al., 2010b). This may be related to the generally large lamellae of elasmobranchs (a thicker lamellar epithelium would provide additional support) or other functions associated with individual epithelial components. For example, Hughes and Wright (1970) showed that benthic elasmobranchs have a thicker lamellar

basement membrane and generally longer microvilli (which would anchor a thicker mucosal layer on the gills) than those of teleosts. Both could be related to reducing the loss of important ions and other molecules to the external environment that are used by marine elasmobranchs to maintain an osmolarity close to that of seawater (Smith, 1936). This is in part supported by the findings of Fines et al. (2001) that showed that the basolateral membranes of the gill epithelial cells of *S. acanthias* have a very high cholesterol content that likely lowers gill permeability to urea without inhibiting oxygen diffusion, and findings by Hill et al. (2004) showing the low permeability of urea and other molecules through the gill apical membrane and mucous layer. Third, in addition to a thicker water–blood barrier, the blood channels of elasmobranch lamellae are generally wider (thus increasing lamellar thickness and diffusion distances within the blood), likely to accommodate the intrinsically large red blood cells of elasmobranchs (Fänge, 1992; Wilhelm Filho et al., 1992).

6.4. Scaling

Important insight into gill function and whole organismal physiology can be gained by examining how gill dimensions change with fish growth. This relationship is typically described by the power-law scaling equation:

$$Y = aM^b \tag{3.5}$$

or log form,

$$\log Y = \log a + b \log M \tag{3.6}$$

where, Y is a particular gill morphometric (e.g., A, L_{fil}, n_{lam}, or A_{lam}), a is the intercept value for a 1 g specimen, M is fish mass, and b is the species-specific slope or scaling exponent. Assuming the gills grow isometrically (i.e., gill mass increases at the same rate as body mass, b=1.0), isometric geometry of the gills (the length/area/volume relationship) predicts that L_{fil} should scale to the one-third (i.e., length/volume, b=0.33), n_{lam} to the negative one-third (length^{-1}/volume, b=−0.33), and A_{lam} to the two-thirds (area/volume, b=0.67), which when added together, sum to the expected scaling exponent for total gill surface area (area/volume, b=0.67).

In teleost fishes, the scaling exponent for gill surface area to body mass can range from under 0.50 to over 1.00, with a mean of 0.80. This mean is significantly greater than that predicted by isometric scaling and appears to correlate with the mean scaling exponent for fish standard metabolic rate with body mass (0.81) (Palzenberger and Pohla, 1992; Wegner, 2011). For the much more limited pool of elasmobranchs studied to date (Table 3.3) the gill area scaling exponent ranges from 0.74 to 1.03 with a mean of 0.85,

Table 3.3

Regression equation intercepts (a) and scaling exponents (b) for elasmobranch gill surface areas (A) shown in Fig. 3.15 and associated componential dimensions (L_{fil}, n_{lam}, and A_{lam}) in comparison to body mass (M, in g) according to the power-law scaling equation $Y=aM^b$

Common name	Species names	A (cm^2)		L_{fil} (cm)		n_{lam} (mm^{-1})		A_{lam} (mm^2)		Mass range (kg)	Reference
		a	b	a	b	a	b	a	b		
Common thresher shark	*Alopias vulpinus*	2.46	1.0299	499.16	0.3216	56.71	−0.1628	0.00048	0.8609	7.9–91.5	Wootton et al. (2015)
Small-spotted catshark	*Scyliorhinus canicula*	2.62	0.9610	72.28	0.3510	17.15	−0.0710	0.01030	0.6840	0.115–0.800	Hughes (1972)
Marbled electric ray[+]	*Torpedo marmorata*	1.17	0.9368	51.36	0.3966	34.17	−0.1665	0.00336	0.7060	0.1–20.0	Hughes (1978)
Pelagic thresher shark	*Alopias pelagicus*	12.51	0.8928	774.31	0.2901	78.61	−0.1871	0.00105	0.7881	11.8–78.2	Wootton et al. (2015)
Blue shark	*Prionace glauca*	5.50	0.8800	162.18	0.3800	25.70	−0.0900	0.00661	0.5900	12–120	Emery and Szczepanski (1985)
Dusky shark	*Carcharhinus obscurus*	6.17	0.8800	186.21	0.4000	67.61	−0.1600	0.00245	0.6500	20–200	Emery and Szczepanski (1985)
Shortfin mako	*Isurus oxyrinchus*	35.89	0.7834	612.31	0.2904	39.19	−0.1113	0.00748	0.6043	4.6–71.0	Wegner et al. (2010b)
Nursehound	*Scyliorhinus stellaris*	6.21	0.7790	81.40	0.3650	30.27	−0.1670	0.01270	0.5800	0.585–2.615	Hughes et al. (1986)
Bigeye thresher shark	*Alopias superciliosus*	52.17	0.7753	2036.74	0.2221	107.87	−0.2154	0.00092	0.7921	48.8–127.3	Wootton et al. (2015)
White shark	*Carcharodon carcharias*	42.66	0.7700	954.99	0.2900	56.23	−0.1500	0.00407	0.6300	12–1300	Emery and Szczepanski (1985)
Shortfin mako	*Isurus oxyrinchus*	57.54	0.7400	676.08	0.2800	100.00	−0.2000	0.00427	0.6600	12–125	Emery and Szczepanski (1985)
Sandbar shark	*Carcharhinus plumbeus*	24.55	0.7400	134.90	0.4000	46.77	−0.1300	0.01905	0.4800	20–75	Emery and Szczepanski (1985)
Common thresher shark[a]	*Alopias vulpinus*	2511.89	0.4100	263.03	0.3700	457.09	−0.3400	0.10233	0.3800	60–180	Emery and Szczepanski (1985)
Atlantic stingray[a]	*Dasyatis sabina*	421.46	0.2000							0.40–0.65	Grim et al. (2012)
Cownose ray[a]	*Rhinoptera bonasus*	2987.61	0.2000							4.5–7.2	Grim et al. (2012)
	Mean		**0.8474**		**0.3322**		**−0.1509**		**0.6688**		

[a]Indicates species not included in scaling exponent means due to low sample size or a limited body-mass size range in comparison to other species. [+]Five of the 22 specimens included in the regression equations for *Torpedo marmorata* are the electric ray, *T. nobiliana*. L_{fil}, total filament length; n_{lam}, lamellar frequency (=number of lamellar per mm filament); A_{lam}, mean bilateral surface area of a lamella.

which closely matches the mean scaling exponent for standard/resting metabolic rate (0.84) in six elasmobranch species for which mass dependent metabolic data are available (Hughes, 1978; Du Preez et al., 1988; Sims, 1996; Ezcurra, 2001; Dowd et al., 2006). Species-specific deviation from the mean gill-area-to-body-mass scaling exponent may provide insight into changes in fish metabolism or other physiological processes with growth. For example, the high scaling exponent for the gill surface area of the common thresher shark, *Alopias vulpinus* (1.03), may reflect an increased ability for regional endothermy (and hence disproportionate increase in oxygen demands) with body size (Wootton et al., 2015). This disproportionate increase in gill surface area results from a disproportionate increase in the size of gill lamellae (the scaling exponent for A_{lam} is 0.86 in comparison to the predicted 0.67) (Table 3.3), which is consistent with theoretical predictions for augmenting gill area while minimizing increases to gill resistance.

6.5. Adaptations for Fast Swimming

Within the apparent constraints imposed on elasmobranch gill dimensions (see Section 6.3), fast swimming pelagic sharks have much larger gill surface areas and shorter diffusion distances than those of benthic species (Fig. 3.15, Table 3.2). In the lamnids and some other oceanic groups, the pectoral fins are positioned more posteriorly than in many less-active benthic species (Thompson and Simanek, 1977; Compagno, 1990; Dolce and Wilga, 2013). While this positioning likely has hydrodynamic considerations for continuous swimming, it may also allow for the longitudinal expansion of the branchial chambers and generally longer gill filaments. Fast-swimming pelagic sharks also tend to have relatively large gill slits of similar length (Dolce and Wilga, 2013), which likely minimizes slit effects on branchial resistance and swimming drag. While fast-swimming sharks lack the gill fusions of ram-ventilating teleosts [used to stabilize the gill filaments and lamellae against a forceful ram-ventilatory stream (Muir and Kendall, 1968; Wegner et al., 2013)], their filaments are strengthened by the interbranchial septum and their lamellae appear to be stiffened by lamellar vascular sacs (see Section 5.1).

The largest gill areas in all elasmobranchs are found in the lamnid and alopiid sharks and can be more than twice those of other oceanic shark species (Emery and Szczepanski, 1986; Wegner et al., 2010b; Wootton et al., 2015). For lamnids and *A. vulpinus*, large gill areas are likely required to meet high oxygen demands associated with regional endothermy and increased aerobic performance. However, the gill surface area of the pelagic thresher shark, *A. pelagicus*, which is not known to elevate its body temperature above ambient (Patterson et al., 2011), rivals that of the

regionally endothermic lamnids and *A. vulpinus* (Fig. 3.15). Wootton et al. (2015) suggested that the large gill area in *A. pelagicus* may, in part, reflect its tropical warm-water environment, which contains less oxygen than temperate seas (warm water has a reduced oxygen solubility coefficient) and would keep the body temperature of *A. pelagicus* above that of most regionally endothermic sharks. As most studies have focused on temperate and subtropical species, there is little known about the gill dimensions of warmer water elasmobranchs and how gill morphometrics and structure may vary with temperature.

6.6. Adaptations for Hypoxia

Large gill surface areas also allow for enhanced oxygen uptake in hypoxic environments. The largest elasmobranch gill surface area documented to date belongs to the bigeye thresher shark, *Alopias superciliosus* (Wootton et al., 2015), which undertakes diel vertical migrations to depths of 300–500 m where, in many locations within its range, it forages within the hypoxic waters of the subsurface oxygen minimum zone (OMZ) (Nakano et al., 2003; Weng and Block, 2004). The gill area of the bigeye thresher is increased by its extremely long gill filaments, which occur within laterally expanded branchial chambers (Fig. 3.17A). The large size of these brachial chambers emphasizes the nuchal grooves along the sides of the head and produces its distinct "helmeted" contour. Wootton et al. (2015) suggested that as *A. superciliosus* feeds heavily on slow-moving prey within the OMZ, the selective pressure of cranial streamlining may have been relaxed, thus allowing for larger branchial chambers capable of housing a gill surface area larger than those of other, more streamlined elasmobranchs.

Other deep-water sharks that occupy the OMZ appear to have a similar approach to augment gill surface area through long filaments, although gill morphometric data are needed to confirm this. Some species of the deep-water catshark genus *Parmaturus* and the triakid genus *Iago* are reported to have enlarged branchial chambers and elongated gill filaments (Compagno, 1990). The lollipop catshark, *Cephalurus cephalus*, found at depths of 250–850 m gets its name from its unique body shape and large head which likely houses expanded branchial chambers and gills (Fig. 3.17B). In addition to having an extra gill arch, the deep-dwelling frill shark (240–1500 m) possesses gill filaments that appear to fill the branchial cavities and are long enough to extend out their large gill slits. The extension of filament tips out of the gill slits has also been suggested for the deep-dwelling *Apristurus* catsharks (Graham, 2006). However, this seems unlikely due to the small gill slits of this genus, which if filled with filaments, would likely obstruct

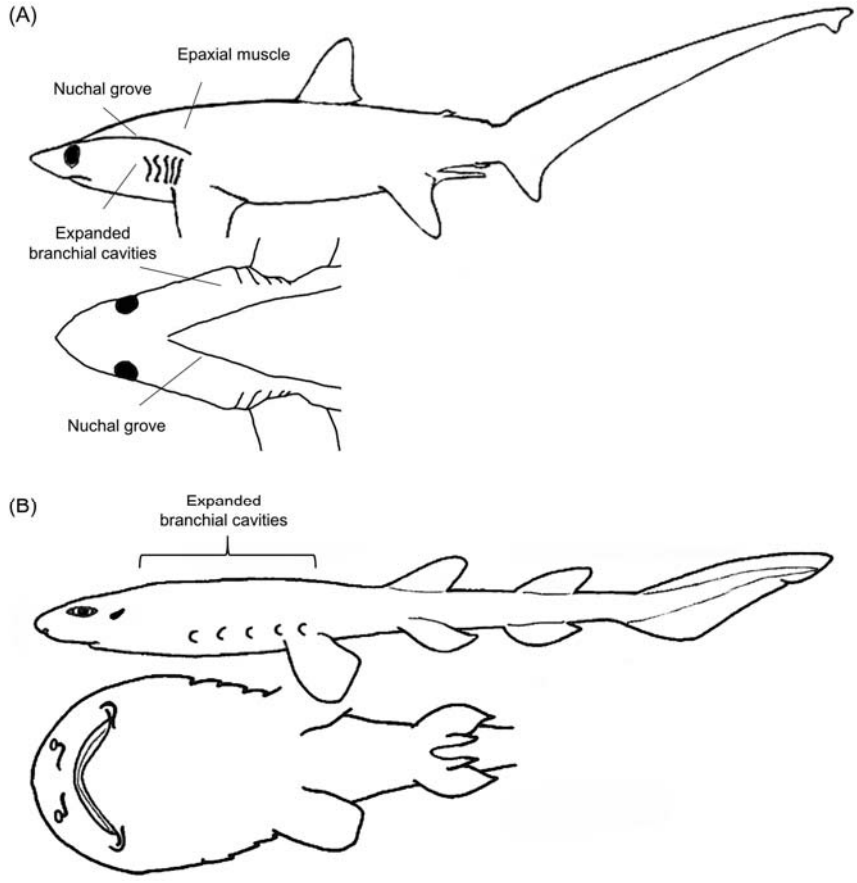

Figure 3.17. Expanded branchial chambers of the (A) bigeye thresher, *Alopias superciliosus*, and (B) lollipop catshark, *Cephalurus cephalus* which house large gills for increased gas exchange within the oxygen minimum zone. The branchial chambers are expanded laterally in *A. superciliosus* and both laterally and longitudinally in *C. cephalus*. Images modified from or based on Compagno (1990, 2001) and Wootton et al. (2015).

ventilatory flow. Furthermore, specimens examined by the current author in the preparation of this chapter did not possess this particular anatomy.

Recent research has shown that at least some elasmobranchs are capable of relatively rapid increases in gill surface area in response to decreases in environmental dissolved oxygen. Shallow marine and estuarine species such as the Atlantic stingray, *Dasyatis sabina*, can become trapped in shallow isolated pools during low tide that, at night, can become severely hypoxic due to biological respiration. Dabruzzi and Bennett (2013) showed

that stingrays in the laboratory exposed to daily hypoxic intervals (30% O_2 saturation for 7 h), increased gill surface by up to 70% after just 20 days. Like many freshwater teleosts (see for review Nilsson, 2013), this appears to occur primarily via apoptosis of the filament epithelium which exposes additional lamellar area that is embedded within the filament body (Bennett, Personal Communication). However, detailed morphometric analyses are still needed and the wide range of gill surface areas reported for this species (see Fig. 3.15) (Grim et al., 2012; Dabruzzi and Bennett, 2013) suggests that even larger changes or population-specific differences in gill surface area are likely. Additional studies on changes in gill morphology in this and other species such as the epaulette shark, *Hemiscyllium ocellatum* (which is often exposed to anoxic pools in tropical reefs) would provide further valuable insight into elasmobranch respiratory plasticity and responses to hypoxia.

6.7. Adaptations for Freshwater

Although the vast majority of elasmobranchs occur solely in the marine environment, approximately 5% of extant species can regularly be found in freshwater, and a few groups (comprising about 3–4% of elasmobranch species) such as the potamotrygonid stingrays, are specialized for freshwater and cannot tolerate higher salinities (Ballantyne and Robinson, 2010). Most of the physiological research on freshwater elasmobranchs has focused on their ability to osmoregulate, which, with the typical marine elasmobranch osmolarity close to that of seawater, requires a number of adaptations. Studies on the gills of freshwater elasmobranchs have focused primarily on the function, prevalence, and distribution of MRCs. For euryhaline species such as *D. sabina* and the bull shark, *Carcharhinus leucas*, MRC abundance increases in freshwater to meet augmented demands for NaCl uptake and acid-base balance (Piermarini and Evans, 2000; Piermarini and Evans, 2001; Reilly et al., 2011). Fig. 3.18 shows the stepwise change in the proliferation and distribution of two MRC subtypes (Na^+/K^+-ATPase-rich and V-H^+-ATPase rich cells) in *D. sabina* that are found primarily in the interlamellar filament epithelium in seawater acclimated individuals, but become increasingly more abundant on the lamellar epithelium with lower salinities (Piermarini and Evans, 2001).

The increase in MRC abundance in the lamellar epithelium for freshwater elasmobranchs likely increases the thickness of the water–blood barrier, thus decreasing the diffusion capacity of the gills (although this and other gill morphometric data are largely lacking from the literature). As air-saturated freshwater typically contains 15–20% more oxygen than seawater (depending on temperature) a thick water–blood barrier may not

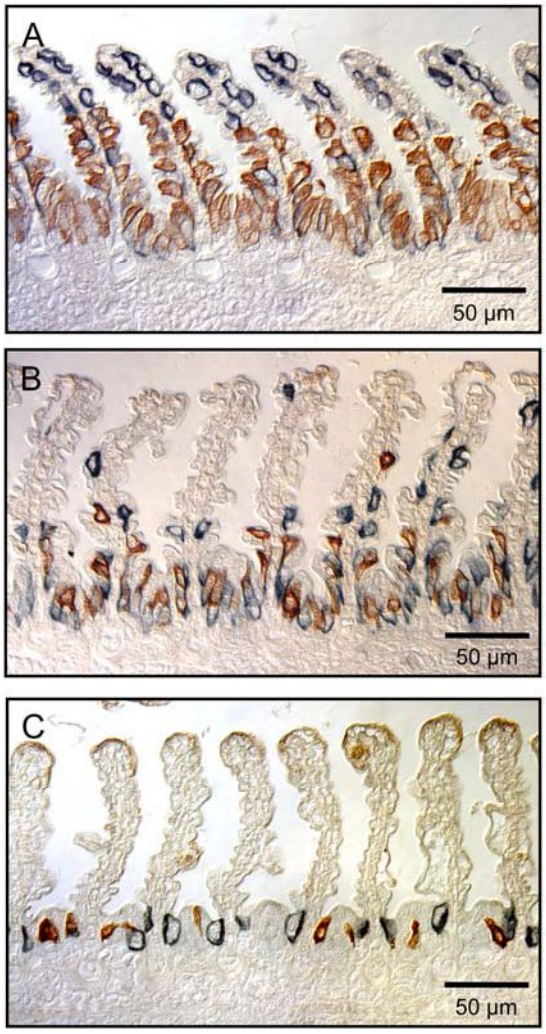

Figure 3.18. Longitudinal sections through the gill filament and lamellae of the Atlantic stingray, *Dasyatis sabina*, showing the relative distribution of mitochondrion-rich cells (brown=V-H^+-ATPase-rich; blue=Na^+/K^+-ATPase-rich) for rays from (A) freshwater, (B) freshwater acclimated to seawater for two weeks, and (C) seawater. Modified from Piermarini and Evans (2001).

be detrimental to oxygen uptake and should be advantageous in decreasing the diffusive loss of ions to the environment. Palzenberger and Pohla (1992) showed that freshwater teleosts have generally smaller gill surface areas than comparable marine teleosts, and this likely correlates to the higher oxygen

concentration in freshwater. Future studies on freshwater elasmobranch morphometrics would provide interesting insight into the osmo-respiratory compromise.

6.8. Adaptations for Feeding – Gill Rakers

One highly variable structural element of the gills not directly associated with gas exchange is the gill raker. In most elasmobranchs, gill rakers are either absent or are small and knob-like and likely serve to protect the gills during feeding. However, four elasmobranch lineages (Cetorhinidae, Megachasmidae, Mobulidae, and Rhincodontidae) have independently evolved elaborate raker-based filtering apparatuses for suspension feeding. Perhaps the most intricate filtration system is found in the whale shark, *Rhincodon typus*, in which nearly the entire pharyngeal surface is lined by 20 giant interconnected filter pads composed of a denticle-covered reticulated mesh with small irregularly shaped pores (Fig. 3.19) (Motta et al., 2010). Each pad, formed by rakers on each gill arch epi- or ceratobranchial, is joined to the neighboring pad by a connective tissue-based raphe (Fig. 3.19B), thus ensuring that all water entering the mouth passes through the filtering apparatus. The reticulated mesh (Fig. 3.19C, D, and F) appears composed of tertiary and quaternary folds of the gill rakers that have fused together to form an irregular pattern. The primary and secondary rakers [termed secondary and primary vanes, respectively, by Motta et al. (2010)] that support the reticulated mesh, appear positioned to help direct post-filter flow toward the gill filaments (Fig. 3.19E and F).

Functionally similar to the filter pads of *R. typus* are the gill rakers of the mobulids (mantas and devil rays), in which individual rakers (also termed filter lobes) contain leaf-like secondary rakers or lobes that are in such close proximity they form a reticulating mesh and assume a plate-like appearance (Fig. 3.20) (Paig-Tran et al., 2013; Paig-Tran and Summers, 2014). Although each row of rakers on either side of each epi- and ceratobranchial is called a filter pad or plate, mobulid pads differ from those of *R. typus* in that they are composed of individual rakers that, with the exception of *Mobula tarapacana*, do not appear to be fused and in no cases connect to the rakers of the opposing arch. However, like *R. typus*, the trailing (water-exit) edge of the primary and secondary rakers form vanes that direct post-filtered water toward the gill filaments for gas exchange (Fig. 3.20B). The orientation and reticulating mesh morphology of the filter pads of both mobulids and *R. typus*, coupled with the finding of prey smaller than mesh size in the stomachs, suggests that both groups may use cross-flow filtration, in which the tangential shearing of water flow parallel to the filter surface pushes particulate food items toward the back of the pharynx to be swallowed

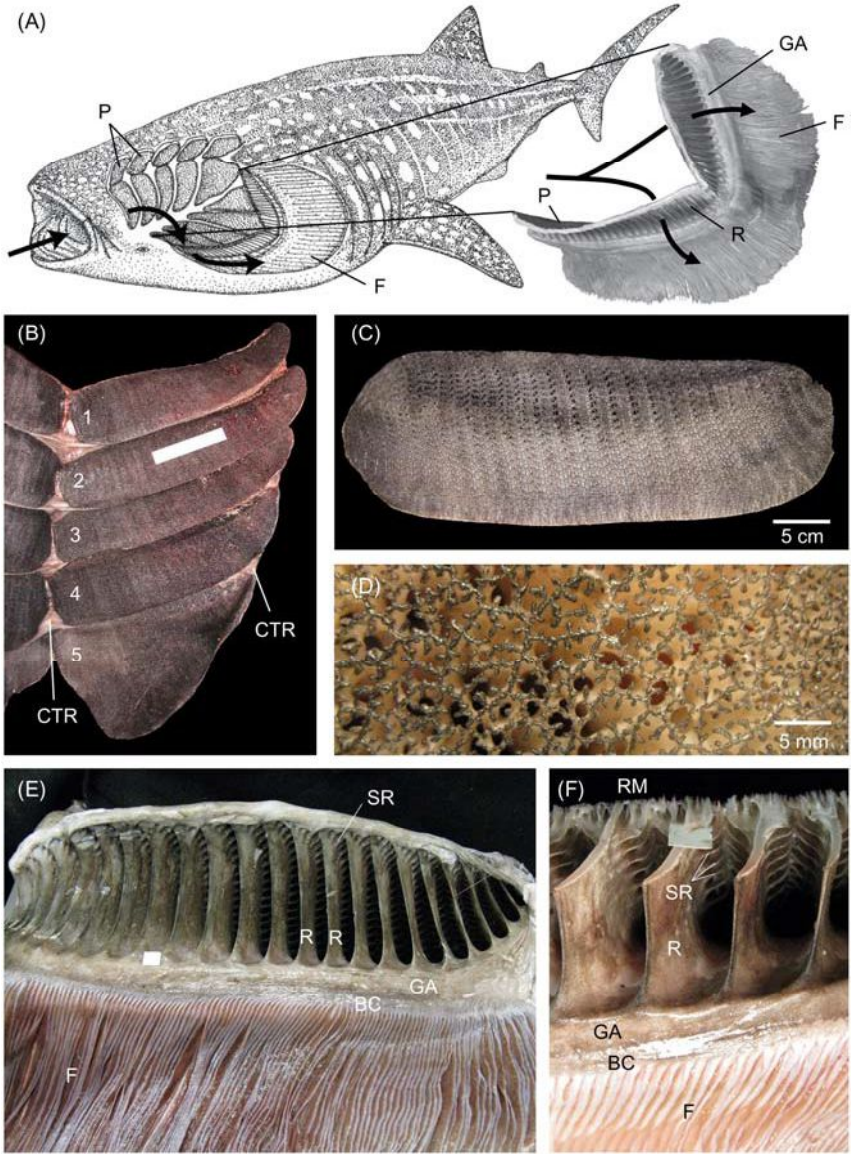

Figure 3.19. The branchial filtering apparatus of the whale shark, *Rhincodon typus*. (A) Schematic rendering of an anterior-lateral view of a whale shark showing the position of the filter pads and direction of water flow as indicated by solid black lines. The enlarged view of a single gill arch shows primarily the trailing (water-exit) edge of the filter pad revealing the primary gill rakers that provide structural support and direct flow toward the gill filaments. (B) Water-entry side of the upper (left) and lower (right) filter pads from the left side of the orobranchial chamber removed from the gill arches and laid flat. Note the connective tissue-

without direct contact with the sieve (Motta et al., 2010; Paig-Tran et al., 2013; Paig-Tran and Summers, 2014).

The gill rakers of the basking shark, *Cetorhinus maximus*, and megamouth shark, *Megachasma pelagios*, are much simpler in structure and are likely associated with a more traditional filtering mechanism in which the food items become physically caught in the rakers for collection and later swallowing. For *C. maximus*, the rakers are long and largely rigid keratinous bristle-like structures (Fig. 3.21A) that emanate from the distal end on both sides of each gill arch (Daniel, 1934; Matthews and Parker, 1950; Sims, 2008). When the mouth is closed, the rakers lay flat against the arch. As the mouth opens for feeding, the rakers extend off the gill arch and approach those of the adjacent arch, forming a series of "V" shaped filters that point toward the oral cavity and fill the pharyngeal slits (Daniel, 1934; Sims, 1996). A thick mucosal epithelium lines much of the gill arches and orobranchial cavity and likely produces mucus that in theory coats the rakers to aid in prey adhesion and capture (Matthews and Parker, 1950; Paig-Tran and Summers, 2014). In *M. pelagios*, closely spaced, repeating, and largely flexible papillae-like rakers (Fig. 3.21B and C) are composed of a hyaline cartilage core covered by dense connective tissue, a thin epithelial layer, and placoid denticles (Yano et al., 1997; Paig-Tran and Summers, 2014). The functional significance of the numerous denticles (Fig. 3.21C) is not known, but like *C. maximus*, it is hypothesized that they may be largely covered by mucus for prey adhesion. While *M. pelagios* feeding has never been observed, the large mouth and small gill slits suggest an engulfment mechanism (in which engulfed prey are filtered as water is pushed out the gill slits) rather than the steady swimming, ram filtration that is used heavily by *R. typus* and likely exclusively by mobulids and *C. maximus*.

based raphae connecting adjacent gill pads to ensure all water passes through the filtering apparatus. Gill pads are numbered from 1–5 anterior to posterior. The white ruler is 15 cm. (C) Enlarged view of the water-entry side of a gill pad showing the reticulated mesh. (D) Enlarged view of the reticulated mesh. (E) Water-exit side of the gill pad revealing the primary and secondary rakers [secondary and primary vanes respectively of Motta et al. (2010)] that support the gill pads and direct water toward the gill filaments. (F) Magnified view of a cross-section though the gill pad showing the reticulated mesh which appears to be composed of tertiary and quaternary folds of the gill rakers that have fused together. The white square in (E and F) is 1.0 cm^2. Water flow through the filter in (B–D) is into the page and is from top to bottom in (E and F). BC, branchial canopy; CTR, connective tissue raphe; F, filaments; GA, gill arch; P, filter pad; R, primary raker; RM, reticulated mesh; SR, secondary raker. (A–C, E, and F) Modified from Motta et al. (2010) and (D) Courtesy of P. Motta (Unpublished). (A) Based on an illustration by Emily S. Damstra.

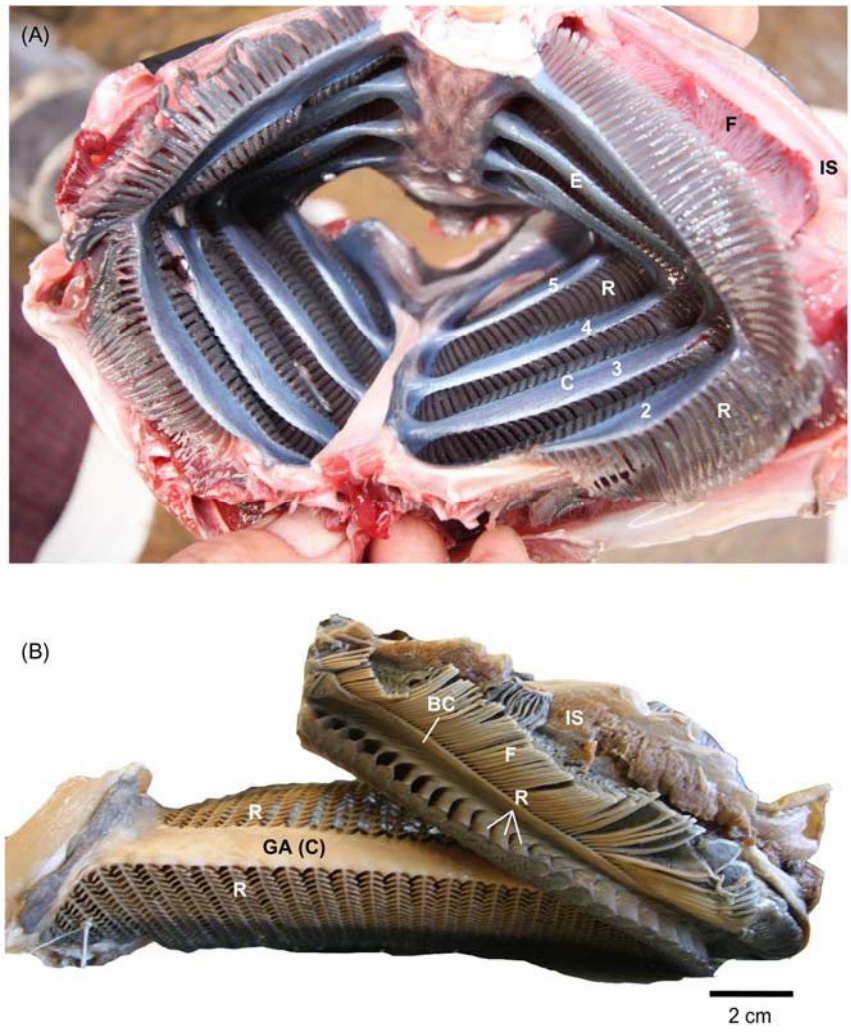

Figure 3.20. Gill filtering apparatus of the mobulid rays. (A) Anterior view into the orobranchial cavity of the spinetail mobula, *Mobula japonica*, showing the leading (water-entry) side of the gill rakers emanating from both sides of each gill arch. Gill arches 2–5 are numbered. (B) Extracted gill arch from the Chilean devil ray, *M. tarapacana*, showing the leading surface of the primary and secondary rakers from the ceratobranchial (lower left) and the outflow channels of the rakers from the epibranchial (upper right). BC, branchial canopy; C, ceratobranchial; E, epibranchial; F, filaments; GA, gill arch; IS, interbranchial septum; R, raker. (A) Reprinted with permission of Gisela Kaufmann, Manta Trust. (B) Modified from Paig-Tran et al. (2013).

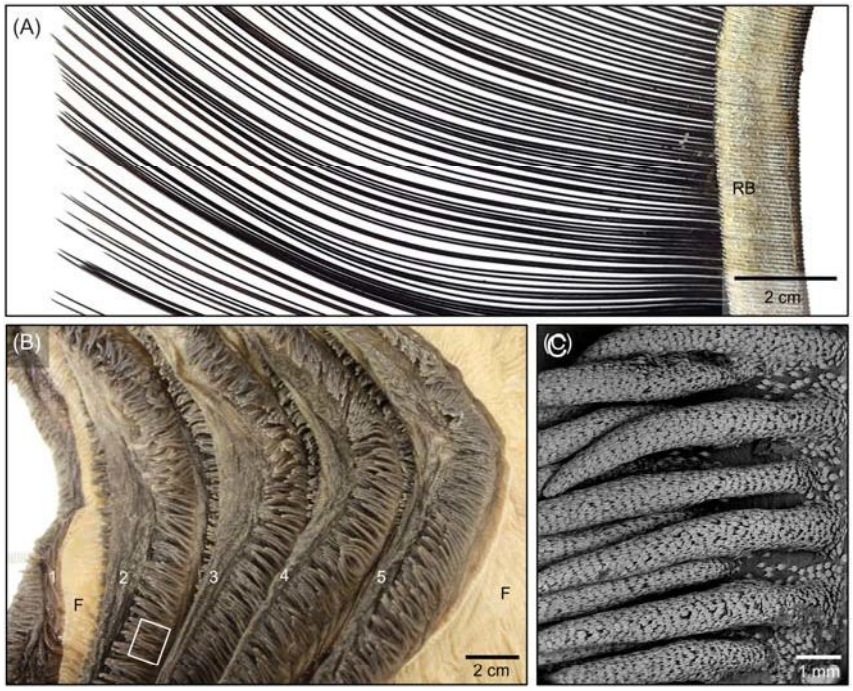

Figure 3.21. Gill rakers of the (A) basking shark, *Cetorhinus maximus* and (B and C) megamouth shark, *Megachasma pelagios.* The long bristle-like gill rakers of *C. maximus* (A), which interconnect at their base, are shown removed from the gill arch. The papillae-like gill rakers for *M. pelagios* (B) are shown emanating from both sides of each arch (numbered 1–5). (C) is a magnified scanning electron micrograph of the white box in (B) showing the denticles that cover the surface of *M. pelagios* rakers. F, filaments; RB, raker base.

7. CONCLUSIONS

As in other fishes, the gills of elasmobranchs are essential in gas exchange, ion and pH balance, and nitrogen excretion, and, in some cases, feeding. Despite the importance of the gill to basic physiological function, most of our knowledge on elasmobranch gill structure and function has historically been based on the study of just a few representative species such as *S. acanthias*, *S. canicula*, and *S. stellaris*, which are relatively common, sedentary, and temperate sharks that are easily held in captivity. It has only been more recently that morphological assessments have been expanded to include a wider diversity of elasmobranch species to those that push the limits of physiological function in terms of rapid swimming and regional

endothermy (Wegner et al., 2010b, 2012), life in hypoxia (Dabruzzi and Bennett, 2013; Wootton et al., 2015), or adaptations for freshwater (Piermarini and Evans, 2000, 2001; Duncan et al., 2010; Reilly et al., 2011). Such research is yielding exciting results and insights into the capabilities and limitations of the elasmobranch gill for gas exchange and consequently aerobic function, gill plasticity and possible remodeling, and adaptations for extreme osmotic stress. Still these studies have likely just begun to scratch the surface. The gill morphology of many groups such as deep-sea and obligate freshwater elasmobranchs has gone largely unstudied. Unfortunately, due to their large body size, extreme or remote habitats, and active swimming requirements, many elasmobranch groups cannot be brought into the laboratory for direct physiological study. For such species, examination of branchial morphology can provide insight into metabolic requirements and other important physiological processes.

ACKNOWLEDGMENTS

I would like to thank G. Kaufman, P. J. Motta, K. R. Olson, E. W. M. Paig-Tran, P. M. Piermarini, J. Roa, M. Tresguerres, and J. M. Wilson for providing images used in figures for this chapter. I also thank H. Dewar, H. J. Walker, and the Scripps Institution of Oceanography Vertebrate Collection for specimens and samples examined, and E. York and S. Faulhaber for technical assistance with SEM use. Finally, I thank H. Aryafar, H. Dewar, and an external reviewer for their helpful comments on the manuscript.

REFERENCES

Acrivo, C. (1935a). Sur l'organisation et la structure du corps caverneux chez *Scyllium canicula* Cuv. *Bull. Histol. Appl. Physiol. Path.* **12**, 362–372.

Acrivo, C. (1935b). Über die Neubildung von Kiemenlamellen bei *Scyliium canicula*. *Cuv. Zool. Anz.* **109**, 173–176.

Ballantyne, J. S. and Robinson, J. W. (2010). Freshwater elasmobranchs: a review of their physiology and biochemistry. *J. Comp. Physiol. B.* **180**, 475–493.

Basten, B. L., Sherman, R. L., Lametschwandtner, A. and Spieler, R. E. (2011). Development of embryonic gill vasculature in the yellow stingray, *Urobatis jamaicensis*. *Anat. Rec.* **294**, 1423–1432.

Benz, G. W. (1984). On the conservative nature of the gill filaments of sharks. *Environ. Biol. Fishes* **10**, 111–116.

Bernal, D., Carlson, J. K., Goldman, K. J. and Lowe, C. G. (2012). Energetics, metabolism, and endothermy in sharks and rays. In *Biology of Sharks and Their Relatives* (eds. J. C. Carrier, J. A. Musick and M. R. Heithaus), second ed., pp. 211–237. Boca Raton, FL: CRC Press.

Bhargava, V., Lai, N. C., Graham, J. B., Hempleman, S. C. and Shabetai, R. (1992). Digital image analysis of shark gills: modeling of oxygen transfer in the domain of time. *Am. J. Physiol.* **263**, R741–R746.

Boylan, J. W. and Lockwood, M. (1962). Urea and thiourea excretion by dogfish kidney and gill: effect of temperature. *Bull. Mt. Desert Isl. Biol. Lab. 4*, 25.

Brainerd, E. L. and Ferry-Graham, L. A. (2006). Mechanics of respiratory pumps. In *Fish Physiology: Fish Biomechanics*, Vol. 23 (eds. R. E. Shadwick and G. V. Lauder), pp. 1–28. San Francisco, LA: Academic Press.

Brett, J. R. and Blackburn, J. M. (1978). Metabolic rate and energy expenditure of the spiny dogfish, *Squalus acanthias*. *J. Fish. Res. Bd. Can.* **35**, 816–821.

Brown, C. E. and Muir, B. S. (1970). Analysis of ram ventilation of fish gills with application to skipjack tuna (*Katsuwonus pelamis*). *J. Fish. Res. Bd. Can.* **27**, 1637–1652.

Butler, P. J. (1999). Respiratory system. In *Sharks, Skates and Rays: The Biology of Elasmobranch Fishes* (ed. W. C. Hamlett), pp. 174–197. Baltimore, MD: Johns Hopkins University Press.

Butler, P. J. and Metcalfe, J. D. (1988). Cardiovascular and respiratory systems. In *Physiology of Elasmobranch Fishes* (ed. T. J. Shuttleworth), pp. 1–47. Berlin: Springer-Verlag.

Cameron, J. N., Randall, D. J. and Davis, J. C. (1971). Regulation of the ventilation-perfusion ratio in the gills of *Dasyatis sabina* and *Squalus suckleyi*. *Comp. Biochem. Physiol.* **39A**, 505–519.

Clark, E. and Kabasawa, H. (1976). Factors affecting the respiration rates of two Japanese sharks, dochizame (*Triakis scyllia*) and nekozame (*Heterodontus japonicus*). *Keikyu Aburatsubo Marine Park Aquarium Ann. Rep.* **7/8**, 14–26.

Compagno, L. J. V. (1990). Alternative life-history styles of cartilaginous fishes in time and space. *Environ. Biol. Fishes* **28**, 33–75.

Compagno, L. J. V. (2001). *Sharks of the World. An Annotated and Illustrated Catalogue of Shark Species Known to Date. Volume 2. Bullhead, Mackerel and Carpet Sharks (Heterodontiformes, Lamniformes and Orectolobiformes)*. Rome: FAO.

Cooke, I. R. C. (1980). Functional aspects of the morphology and vascular anatomy of the gills of the endeavour dogfish, *Centrophorus scalpratus* (McCulloch) (Elasmobranchii: Squalidae). *Zoomorphologie* **94**, 167–183.

Crespo, S. (1982). Surface morphology of dogfish (*Scyliorhinus canicula*) gill epithelium, and surface morphological changes following treatment with zinc sulfate: a scanning electron microscope study. *Mar. Biol.* **67**, 159–166.

Dabruzzi, T. F. and Bennett, W. A. (2013). Hypoxia effects on gill surface area and blood oxygen-carrying capacity of the Atlantic stingray, *Dasyatis sabina*. *Fish Physiol. Biochem.* **40**, 1011–1020.

Daniel, J. F. (1934). *The Elasmobranch Fishes*. Berkeley: University of California Press.

Daniel, T. L. (1981). Fish mucus: *in situ* measurements of polymer drag reduction. *Biol. Bull.* **160**, 376–382.

De Vries, R. and De Jager, S. (1984). The gill in the spiny dogfish, *Squalus acanthias*: respiratory and nonrespiratory function. *Am. J. Anat.* **169**, 1–29.

Dolce, J. L. and Wilga, C. D. (2013). Evolutionary and ecological relationships of gill slit morphology in extant sharks. *Bull. Mus. Comp. Zool.* **161**, 79–109.

Donald, J. A. (1989). Vascular anatomy of the gills of the stingarees *Urolophus mucosus* and *U. paucimaculatus* (Urolophidae, Elasmobranchii). *J. Morphol.* **200**, 37–46.

Dowd, W. W., Brill, R. W., Bushnell, P. G. and Musick, J. A. (2006). Standard and routine metabolic rates of juvenile sandbar sharks (*Carcharhinus plumbeus*), including the effects of body mass and acute temperature change. *Fish. Bull.* **104**, 323–331.

Duncan, W. P., Silva, N. F. and Fernandes, M. N. (2011). Mitochondrion-rich cells distribution, Na^+/K^+-ATPase activity and gill morphometry of the Amazonian freshwater stingrays (Chondrichthyes: Potamotrygonidae). *Fish Physiol. Biochem.* **37**, 523–531.

Duncan, W. P., Costa, O. T. F., Sakuragui, M. M. and Fernandes, M. N. (2010). Functional morphology of the gill in Amazonian freshwater stingrays (Chondrichthyes: Potamotrygonidae): Implications for adaptation to freshwater. *Physiol. Biochem. Zool.* **83**, 19–32.

Dunel, S. and Laurent, P. (1980). Functional organisation of the gill vasculature in different classes of fish. In *Epithelial Transport in the Lower Vertebrates* (ed. B. Lahlou), pp. 37–58. Cambridge: Cambridge University Press.

Du Preez, H. H., McLachlan, A. and Marais, J. F. K. (1988). Oxygen consumption of two nearshore marine elasmobranchs, *Rhinobatos annulatus* (Muller & Henle, 1841) and *Myliobatus aquila* (Linnaeus, 1758). *Comp. Biochem. Physiol.* **89A**, 283–294.

Emery, S. H. and Szczepanski, A. (1986). Gill dimensions in pelagic elasmobranch fishes. *Biol. Bull.* **171**, 441–449.

Evans, D. H., Piermarini, P. M. and Choe, K. P. (2004). Homeostasis: osmoregulation, pH regulation, and nitrogen excretion. In *Biology of Sharks and Their Relatives* (eds. J. C. Carrier, J. A. Musick and M. R. Heithaus), pp. 247–268. Boca Raton, FL: CRC Press.

Evans, D. H., Piermarini, P. M. and Choe, K. P. (2005). The multifunctional fish gill: dominant site of gas exchange, osmoregulation, acid-base regulation, and excretion of nitrogenous waste. *Physiol. Rev.* **85**, 97–177.

Ezcurra, J.M., 2001. The Mass-Specific Routine Metabolic Rate of Captive Pelagic Stingrays, *Dasyatis violacea*, with Comments on Energetics. Master's thesis. California State University, Moss Landing Marine Laboratory, Stanislaus. p. 86.

Fänge, R. (1992). Fish blood cells. In *Fish Physiology: The Cardiovacular System*, vol. 12B (eds. R. S. Hoar, D. J. Randall and A. P. Farrell), pp. 1–54. San Diego, CA: Academic Press.

Farrell, A. P., Sobin, S. S., Randall, D. J. and Crosby, S. (1980). Intralamellar blood flow patterns in fish gills. *Am. J. Physiol.* **239**, R428–R436.

Fines, G. A., Ballantyne, J. S. and Wright, P. A. (2001). Active urea transport and an unusual basolateral membrane composition in the gills of a marine elasmobranch. *Am. J. Physiol. Regul. Integr. Comp. Physiol.* **280**, R16–R24.

Goto, T., Shiba, Y., Shibagaki, K. and Nakaya, K. (2013). Morphology and ventilatory function of gills in the carpet shark family Parascylliidae (Elasmobranchii, Orectolobiformes). *Zoolog. Sci.* **30**, 461–468.

Graham, J. B. (2006). Aquatic and aerial respiration. In *The Physiology of Fishes* (eds. D. H. Evans and J. B. Claiborne), third ed., pp. 85–117. Boca Raton, FL: CRC Press.

Grigg, G. C. and Read, J. (1970). Gill function in an elasmobranch. *J. Vergl. Physiol* **29**, 439–451.

Grim, J. M., Ding, A. A. and Bennett, W. A. (2012). Differences in activity level between cownose rays (*Rhinoptera bonasus*) and Atlantic stingrays (*Dasyatis sabina*) are related to differences in heart mass, hemoglobin concentration, and gill surface area. *Fish Physiol. Biochem.* **38**, 1409–1417.

Hildebrand, M. and Goslow, G. (2001). *Analysis of Vertebrate Structure*. New York, NY: John Wiley & Sons.

Hill, W. G., Mathai, J. C., Gensure, R. H., Zeidel, J. D., Apodaca, G., Saenz, J. P., Kinne-Saffran, E., Kinne, R. and Zeidel, M. L. (2004). Permeabilities of the teleost and elasmobranch gill apical membrane: evidence that lipid bilayers alone do not account for barrier function. *Am. J. Physiol. Cell Physiol.* **287**, C235–C242.

Hughes, G. M. (1960a). A comparative study of gill ventilation in marine teleosts. *J. Exp. Biol.* **37**, 28–45.

Hughes, G. M. (1960b). The mechanism of gill ventilation in the dogfish and skate. *J. Exp. Biol.* **37**, 11–27.

Hughes, G. M. (1966). The dimensions of fish gills in relation to their function. *J. Exp. Biol.* **45**, 177–195.

Hughes, G. M. (1972). Morphometrics of fish gills. *Respir. Physiol.* **14**, 1–25.

Hughes, G. M. (1977). Dimensions and the respiration of lower vertebrates. In *Scale Effects in Animal Locomotion* (ed. T. J. Pedley), pp. 57–81. New York, NY: Academic Press.

Hughes, G. M. (1978). On the respiration of *Torpedo marmorata*. *J. Exp. Biol.* **73**, 85–105.
Hughes, G. M. (1984). General anatomy of the gills. In *Fish Physiology: Gills*, vol. 10A (eds. W. S. Hoar and D. J. Randall), pp. 1–72. San Diego, CA: Academic Press.
Hughes, G. M. and Ballintijn, C. M. (1965). The muscular basis of the respiratory pumps in the dogfish (*Scyliorhinus canicula*). *J. Exp. Biol.* **43**, 363–383.
Hughes, G. M. and Morgan, M. (1973). The structure of fish gills in relation to their respiratory function. *Biol. Rev.* **48**, 419–475.
Hughes, G. M. and Wright, D. E. (1970). A comparative study of the ultrastructure of the water-blood pathway in the secondary lamellae of teleost and elasmobranch fishes – benthic forms. *Z. Zellforsch. Mikrosk. Anat.* **104**, 478–493.
Hughes, G. M., Perry, S. F. and Piiper, J. (1986). Morphometry of the gill of the elasmobranch *Scyliorhinus stellaris* in relation to body size. *J. Exp. Biol.* **121**, 27–42.
Kempton, R. T. (1969). Morphological features of functional significance in the gills of the spiny dogfish, *Squalus acanthias*. *Biol. Bull.* **136**, 226–240.
Laurent, P. (1984). Gill internal morphology. In *Fish Physiology: Gills*, vol. 10A (eds. R. S. Hoar and D. J. Randall), pp. 73–183. Orlando, FL: Academic Press.
Lenfant, C. and Johansen, K. (1966). Respiratory function in the elasmobranch *Squalus suckleyi*. *Respir. Physiol.* **1**, 13–29.
Mallatt, J. (1984). Early vertebrate evolution: pharyngeal structure and the origin of gnathostomes. *J. Zool. Lond.* **204**, 169–183.
Malte, H. (1992). Effect of pulsatile flow on gas exchange in the fish gill: theory and experimental data. *Respir. Physiol.* **88**, 51–62.
Matthews, L. H. and Parker, H. W. (1950). Notes on the anatomy and biology of the basking shark *Cetorhinus maximus* (Gunner). *Proc. Zool. Soc. Lond.* **120**, 535–576.
Metcalfe, J. D. and Butler, P. J. (1986). The functional anatomy of the gills of the dogfish (*Scyliorhinus canicula*). *J. Zool. Lond.* **208**, 519–530.
Motta, P. J., Maslanka, M., Hueter, R. E., Davis, R. L., de la Parra, R., Mulvany, S. L., Habegger, M. L., Strother, J. A., Mara, K. R., Gardiner, J. M., Tyminski, J. P. and Zeigler, L. D. (2010). Feeding anatomy, filter-feeding rate, and diet of whale sharks *Rhincodon typus* during surface ram filter feeding off the Yucatan Peninsula, Mexico. *Zoology* **113**, 199–212.
Muir, B. S. and Hughes, G. M. (1969). Gill dimensions for three species of tunny. *J. Exp. Biol.* **51**, 271–285.
Muir, B. S. and Kendall, J. I. (1968). Structural modifications in the gills of tunas and some other oceanic fishes. *Copeia* **1968**, 388–398.
Nakano, H., Matsunaga, H., Okamoto, H. and Okazaki, M. (2003). Acoustic tracking of the bigeye thresher shark *Alopias superciliosus* in the eastern Pacific Ocean. *Mar. Ecol. Prog. Ser.* **265**, 255–261.
Oikawa, S. and Kanda, T. (1997). Some features of the gills of a megamouth shark and a shortfin mako, with reference to metabolic activity. In *Biology of the Megamouth Shark* (eds. K. Yano, J. F. Morrissey, Y. Yabumoto and K. Nakaya), pp. 93–104. Tokyo: Tokai University Press.
Olson, K. R. (2002). Vascular anatomy of the fish gill. *J. Exp. Zool.* **293**, 214–231.
Olson, K. R. and Kent, B. (1980). The microvasculature of the elasmobranch gill. *Cell Tissue Res.* **209**, 49–63.
Paig-Tran, E. W. M. and Summers, A. P. (2014). Comparison of the structure and composition of the branchial filters in suspension feeding elasmobranchs. *Anat. Rec.* **297**, 701–715.
Paig-Tran, E. W. M., Kleinteich, T. and Summers, A. P. (2013). The filter pads and filtration mechanisms of the devil rays: variation at macro and microscopic scales. *J. Morphol.* **274**, 1026–1043.

Palzenberger, M. and Pohla, H. (1992). Gill surface area of water-breathing freshwater fish. *Rev. Fish. Biol. Fish.* **2**, 187–216.
Park, K., Kim, W. and Kim, H.-Y. (2014). Optimal lamellar arrangement in fish gills. *PNAS* **111**, 8067–8070.
Patterson, J. C., Sepulveda, C. A. and Bernal, D. (2011). The vascular morphology and *in vivo* muscle temperatures of thresher sharks (Alopiidae). *J. Morphol.* **272**, 1353–1364.
Piermarini, P. M. and Evans, D. H. (2000). Effects of environmental salinity on Na^+/K^+-ATPase in the gills and rectal gland of a euryhaline elasmobranch (*Dasyatis sabina*). *J. Exp. Biol.* **203**, 2957–2966.
Piermarini, P. M. and Evans, D. H. (2001). Immunochemical analysis of the vacuolar proton-ATPase B-subunit in the gills of a euryhaline stingray (*Dasyatis sabina*): effects of salinity and relation to Na^+/K^+-ATPase. *J. Exp. Biol.* **204**, 3251–3259.
Piiper, J. and Scheid, P. (1984). Model analysis of gas transfer in fish gills. In *Fish Physiology: Gills: Anatomy, Gas Transfer and Acid-Base Regulation*, vol. 10A (eds. W. S. Hoar and D. J. Randall), pp. 229–262. Orlando, FL: Academic Press.
Piiper, J. and Schumann, D. (1967). Efficiency of O_2 exchange in the gills of the dogfish *Scyliorhinus stellaris*. *Respir. Physiol.* **2**, 135–148.
Randall, D., Burggren, W. and French, K. (2002). *Eckert Animal Physiology: Mechanisms and Adaptations* (5th Edition). New York: W. H. Freeman and Company.
Reilly, B. D., Cramp, R. L., Wilson, J. M., Campbell, H. A. and Franklin, C. E. (2011). Branchial osmoregulation in the euryhaline bull shark, *Carcharhinus leucas*: a molecular analysis of ion transporters. *J. Exp. Biol.* **214**, 2883–2895.
Roa, J. N., Munévar, C. and Tresguerres., M. (2014). Feeding induces translocation of vacuolar proton ATPase and pendrin to the membrane of leopard shark (*Triakis semifasciata*) mitochondrion rich gill cells. *Comp. Biochem. Physiol. A* **174**, 29–37.
Roberts, J. L. (1975). Active branchial and ram gill ventilation in fishes. *Biol. Bull.* **148**, 85–105.
Sala, R., Crespo, S., Martin, V. and Castell, O. (1987). Presence of chloride cells in the gill filaments and lamellae of the skate, *Torpedo marmorata*. *J. Fish Biol.* **30**, 357–361.
Satchell, G. H., Hanson, D. and Johansen, K. (1970). Differential blood flow through the afferent branchial arteries of the skate, *Raja rhina*. *J. Exp. Biol.* **52**, 721–726.
Sepulveda, C. A., Graham, J. B. and Bernal, D. (2007). Aerobic metabolic rates of swimming juvenile mako sharks, *Isurus oxyrinchus*. *Mar. Biol.* **152**, 1087–1094.
Sherman, R. L. and Spieler, R. E. (1998). Examination of gill vasculature of yellow stingray, *Urolophus jamaicensis* (Urolophidae), by SEM observations of resin casts. *Ital. J. Zool.* **65**, 431–434.
Shirai, S. (1992). Identity of extra branchial arches of Hexanchiformes (Pisces, Elasmobranchii). *Bull. Fac. Fish. Hokkaido Univ.* **43**, 24–32.
Sims, D. W. (1996). The effect of body size on the standard metabolic rate of the lesser spotted dogfish. *J. Fish Biol.* **48**, 542–544.
Sims, D. W. (2008). Sieving a living: a review of the biology, ecology, and conservation status of the plankton-feeding basking shark *Cetorhinus maximus*. *Adv. Mar. Biol.* **54**, 171–220.
Smith, H. W. (1936). The retention and physiological role of urea in the Elasmobranchii. *Biol. Rev.* **11**, 49–82.
Strother, J. A. (2013). A computational model of flow between the microscale respiratory structures of fish gills. *J. Theor. Biol.* **338**, 23–40.
Summers, A. P. and Ferry-Graham, L. A. (2003). Respiration in elasmobranchs: new models of aquatic ventilation. In *Vertebrate Biomechanics and Evolution* (eds. V. L. Bels, J.-P. Gase and A. Casinos), pp. 87–100. Oxford: BIOS Scientific.
Sundin, L. and Nilsson, S. (2002). Brachial innervation. *J. Exp. Zool.* **293**, 232–248.

Thompson, K. S. and Simanek, D. E. (1977). Body form and locomotion in sharks. *Amer. Zool.* **17**, 343–354.

Tresguerres, M., Parks, S. K., Katoh, F. and Goss, G. G. (2006). Microtubule-dependent relocation of branchial V-H^+-ATPase to the basolateral membrane in the Pacific spiny dogfish (*Squalus acanthias*): a role in base secretion. *J. Exp. Biol.* **209**, 599–609.

Wegner, N. C. (2011). Gill respiratory morphometrics. In *Encyclopedia of Fish Physiology: From Genome to Environment* (eds. A. P. Farrell, J. J. Cech, J. G. Richards and E. D. Stevens), pp. 803–811. Amsterdam: Elsevier.

Wegner, N. C. and Graham, J. B. (2010). George Hughes and the history of fish ventilation: from Du Verney to the present. *Comp. Biochem. Physiol.* **157A**, 1–6.

Wegner, N. C., Sepulveda, C. A., Bull, K. B. and Graham, J. B. (2010a). Gill morphometrics in relation to gas transfer and ram ventilation in high-energy demand teleosts: scombrids and billfishes. *J. Morphol.* **271**, 36–49.

Wegner, N. C., Sepulveda, C. A., Olson, K. R., Hyndman, K. A. and Graham, J. B. (2010b). Functional morphology of the gills of the shortfin mako, *Isurus oxyrinchus*, a lamnid shark. *J. Morphol.* **271**, 937–948.

Wegner, N. C., Lai, N. C., Bull, K. B. and Graham, J. B. (2012). Oxygen utilization and the branchial pressure gradient during ram ventilation in the shortfin mako, *Isurus oxyrinchus*: Is lamnid shark-tuna convergence constrained by elasmobranch gill morphology? *J. Exp. Biol.* **215**, 22–28.

Wegner, N. C., Sepulveda, C. A., Aalbers, S. A. and Graham, J. B. (2013). Structural adaptations for ram ventilation: gill fusions in scombrids and billfishes. *J. Morphol.* **274**, 108–120.

Weng, K. C. and Block, B. A. (2004). Diel vertical migration in the bigeye thresher shark (*Alopias superciliosus*), a species possessing orbital retia mirabilia. *Fish. Bull.* **102**, 221–229.

Wilhelm Filho, D., Eble, G. J., Kassner, G., Caprario, F. X., Dafre, A. L. and Ohira, M. (1992). Comparative hematology in marine fish. *Comp. Biochem. Physiol.* **102A**, 311–321.

Wilson, J. M. and Laurent, P. (2002). Fish gill morphology: inside out. *J. Exp. Zool.* **293**, 192–213.

Wilson, J. M., Randall, D. J., Vogl, A. W. and Iwama, G. E. (1997). Immunolocalization of proton-ATPase in the gills of the elasmobranch, *Squalus acanthias*. *J. Exp. Zool.* **278**, 78–86.

Wilson, J. M., Morgan, J. D., Vogl, A. W. and Randall, D. J. (2002). Branchial mitochondria-rich cells in the dogfish *Squalus acanthias*. *Comp. Biochem. Physiol.* **132A**, 365–374.

Wootton, T. P., Sepulveda, C. A. and Wegner, N. C. (2015). Gill morphometrics of the thresher sharks (genus *Alopias*): correlation of gill dimensions with aerobic demand and environmental oxygen. *J. Morphol.* **276**, 589–600.

Wright, D. E. (1973). The structure of the gills of the elasmobranch, *Scyliorhinus canicula* (L.). *Z. Zellforsch. Mikrosk. Anat.* **144**, 489–509.

Wright, P. A. and Wood, C. M. (2015). Regulation of ions, acid-base and nitrogenous wastes in Elasmobranchs. In: Shadwick, R.E., Farrell, A.P. and Brauner, C. (Eds.). *Physiology of Elasmobranch Fishes: Internal Processes*, vol. 34B.

Yano, K., Goto, M. and Yabumoto, Y. (1997). Dermal and mucous denticles of a female megamouth shark, *Megachasma pelagios*, from Hakata Bay, Japan. In *Biology of the Megamouth Shark* (eds. K. Yano, J. F. Morrissey, Y. Yabumoto and K. Nakaya), pp. 77–91. Tokyo: Tokai University Press.